Journal of Computational Physics 229 (2010) 3623–3651

Contents lists available at ScienceDirect

Journal of Computational Physics

journal homepage: www.elsevier.com/locate/jcp

Optimal time advancing dispersion relation preserving schemes

Manoj K. Rajpoot [a], Tapan K. Sengupta [b,*], Pravir K. Dutt [a]

[a] Department of Mathematics and Statistics, India
[b] Department of Aerospace Engineering, I.I.T., Kanpur, UP, India

ARTICLE INFO

Article history:
Received 17 August 2009
Received in revised form 12 January 2010
Accepted 14 January 2010
Available online 25 January 2010

Keywords:
DRP property
Error propagation
Explicit Runge–Kutta (RK) schemes
Optimized Runge–Kutta (ORK) schemes
Navier–Stokes equations
Lid driven cavity (LDC) problem

ABSTRACT

In this paper we examine the constrained optimization of explicit Runge–Kutta (RK) schemes coupled with central spatial discretization schemes to solve the one-dimensional convection equation. The constraints are defined with respect to the correct error propagation equation which goes beyond the traditional *von Neumann analysis* developed in Sengupta et al. [T.K. Sengupta, A. Dipankar, P. Sagaut, Error dynamics: beyond von Neumann analysis, J. Comput. Phys. 226 (2007) 1211–1218]. The efficiency of these optimal schemes is demonstrated for the one-dimensional convection problem and also by solving the Navier–Stokes equations for a two-dimensional lid-driven cavity (LDC) problem. For the LDC problem, results for $Re = 1000$ are compared with results using spectral methods in Botella and Peyret [O. Botella, R. Peyret, Benchmark spectral results on the lid-driven cavity flow, Comput. Fluids 27 (1998) 421–433] to calibrate the method in solving the steady state problem. We also report the results of the same flow at $Re = 10,000$ and compare them with some recent results to establish the correctness and accuracy of the scheme for solving unsteady flow problems. Finally, we also compare our results for a wave-packet propagation problem with another method developed for computational aeroacoustics.

1. Introduction

Considerable work has been done to improve the performance of numerical methods in solving space–time-dependent problems by developing dispersion relation preserving (DRP) schemes. One of the early attempts was reported in [11,28] and some recent efforts are discussed in [24,25]. A DRP scheme is one that has the numerical and the physical dispersion relation very close to each other. For Fourier spectral methods these two are identical up to the Nyquist limit, while for other discrete methods, closeness between the two can be realized only for some limited range of space and time steps. It is understood that the dispersion relation refers to space–time dependence of the problem. Despite this, in many earlier attempts, DRP methods were obtained by examining the spatial discretization of the first derivative only, by minimizing truncation error that also reduces phase and dispersion error [2,28] indirectly. In [18], compact schemes were characterized for the full-domain by a spectral analysis, with numerical group velocity used to measure dispersion error. But, the numerical dispersion relation was chosen incorrectly following [30]. In [1,12,15,17], space–time discretizations have been considered together to minimize the error between the numerical amplification factor and the true amplification factor. Hu et al. [12], identified a class of low-dissipation and low-dispersion Runge–Kutta (LDDRK) schemes based on this approach. Following the global analysis [18], correct numerical dispersion relation for combined space–time discretization schemes was identified for convection equation in [9,20,21]. These references emphasized the use of neutrally stable schemes for direct numerical simulation (DNS) and acoustics problems (see also [22]). In the present work, space–time discretization has been

* Corresponding author. Tel.: +91 512 2597945; fax: +91 512 2597561.
E-mail addresses: rajpoot@iitk.ac.in (M.K. Rajpoot), tksen@iitk.ac.in (T.K. Sengupta).

0021-9991/$ - see front matter © 2010 Elsevier Inc. All rights reserved.
doi:10.1016/j.jcp.2010.01.018

considered together to minimize dispersion and phase error, while keeping the scheme neutrally stable. Such a scheme would provide ideal DRP property that should be used for DNS and acoustics.

To obtain DRP schemes, linear convection equation is used as a model to represent convection and wave propagation adequately,

$$\frac{\partial u}{\partial t} + c\frac{\partial u}{\partial x} = 0, \quad c > 0. \tag{1}$$

This is a non-dissipative and non-dispersive equation that convects the initial solution to the right at the group velocity (that is equal to the phase speed c due to non-dispersive property). This provides an ideal test-bed to study numerical methods for neutral stability, error propagation and most importantly the dispersion error [23,32]. We briefly state the principles from [9,22,23,30] that helps an error analysis for a DRP scheme. If the unknown u is represented by its bi-lateral Fourier–Laplace transform at the jth node of a uniformly spaced discrete grid with mesh spacing h by, $u(x_j,t) = \int U(k,t)\, e^{ikx_j}\, dk$, then the exact spatial derivative is given by, $\left[\frac{\partial u}{\partial x}\right]_{exact} = \int ikU\, e^{ikx_j}\, dk$. For discrete methods the same spatial derivative u'_j (denoted by a prime) is represented as [14,18],

$$[u'_j]_{numerical} = \int ik_{eq}\, U\, e^{ikx_j}\, dk. \tag{2}$$

In evaluating the first derivative by its discrete representation, $U(k)$ is multiplied by an equivalent wave number (ik_{eq}), instead of the actual wave number (ik). This difference is one source of errors for all discrete computations. The numerical derivative is represented by [18,19], $u'_j = \frac{1}{h}\sum_{l=1}^{N} C_{jl}\, u_l$, where u_l is at the lth node and N is the total number of nodes used for discretization. The constant matrix $[C]$ is the equivalent explicit representation of discrete representation [18] used to evaluate the derivative. In spectral notation, this derivative is written as [18],

$$u'_j = \int \frac{1}{h} \sum C_{jl}\, U\, e^{ik(x_l - x_j)}\, e^{ikx_j}\, dk \tag{3}$$

using (3) in (1) provides,

$$\frac{dU}{U} = -\left[\frac{cdt}{h}\right] \sum_{l=1}^{N} C_{jl}\, e^{ik(x_l - x_j)} \tag{4}$$

where the first factor on the right hand side is the CFL number (N_c). The left hand side can be written in terms of the nodal numerical amplification factor $(G_j = U_j(k, t^{(n+1)})/U_j(k, t^{(n)}))$ and for the four-stage, fourth order Runge–Kutta time integration scheme this is given as [9,23,32],

$$G_j = 1 - A_j + \frac{A_j^2}{2} - \frac{A_j^3}{6} + \frac{A_j^4}{24} \tag{5}$$

where $A_j = N_c \sum_{l=1}^{N} C_{jl}\, e^{ik(x_l - x_j)}$. If the initial condition for Eq. (1) is given by,

$$u(x_j, t=0) = u_j^0 = \int A_0(k)\, e^{ikx_j}\, dk, \tag{6}$$

then the general solution at any arbitrary time is obtained as,

$$u_j^n = \int A_0(k)\, [|G_j|]^n\, e^{i(kx_j - n\beta_j)}\, dk \tag{7}$$

where β_j can be related to the numerical phase speed. In [18,19,30], space and time discretization was considered independently to obtain k_{eq} and ω_N separately. The numerical phase speed was then erroneously written as: $c_N = \omega_N/k_{eq}$, instead of $c_N = \omega_N/k$. General numerical solution of Eq. (1) can be denoted as,

$$u_N = \int A_0(k)[|G|]^{t/\Delta t} e^{ik(x - c_N t)} dk. \tag{8}$$

Actual numerical dispersion relation was given by [20], $\omega_N = kc_N$, while the exact dispersion relation is, $\omega = kc$. Thus, the normalized numerical phase speed and group velocity at the jth node for Eq. (1) is given by [9,20,23],

$$\left[\frac{c_N}{c}\right]_j = \frac{\beta_j}{\omega \Delta t}, \tag{9}$$

$$\left[\frac{V_{gN}}{c}\right]_j = \frac{1}{N_c}\frac{d\beta_j}{d(kh)}. \tag{10}$$

Theoretically, for any numerical computation one must have $|G| = 1$ and for Eq. (1), the group velocity (V_g) must be equal to the phase speed c. If one defines error as $e = u - u_N$, then the governing equation for error is given by [23],

$$\frac{\partial e}{\partial t} + c\frac{\partial e}{\partial x} = -c\left[1 - \frac{c_N}{c}\right]\frac{\partial u_N}{\partial x} - \int \left(\frac{V_{gN} - c_N}{k}\right)\left[\int ik' A_0 [|G|]^{t/\Delta t} e^{ik'(x - c_N t)} dk'\right] dk - \int \frac{Ln|G|}{\Delta t} A_0 [|G|]^{t/\Delta t} e^{ik(x - c_N t)} dk. \tag{11}$$

One notes that Eq. (11) is exact without any approximation – unlike the modified equation approach [26,33] those account for truncation error by collating the approximated terms while discretizing the governing equation. The form of resultant modified equation depends upon the methods of discretization. In contrast, the present equation clubs error based on generic numerical properties. For example, if the numerical scheme is neutrally stable, then the last term on the right hand side of Eq. (11) would not contribute. This establishes the requirement of neutrally stable methods for the minimization of error. The first term on the right hand side of Eq. (11) is due to the mismatch between physical and numerical phase speed amplifying solution gradient and hence this is due to phase error. The second term on the right hand side of Eq. (11) has been expressed earlier [23] in different form. The present form explains it as due to numerical dispersion. Stability analysis of numerical methods developed for linear differential equation by von Neumann and his associates [7,8] assumes the signal and the error to satisfy the same dynamics, due to the linearity of the governing equation. However, Eq. (11) shows that despite the governing equation being linear, the signal and its associated numerical error do not follow the same dynamics. In numerical computations, error terms evolve differently depending upon the method, while the computed signal and error remain interlaced.

In the present work, we have developed a new strategy for optimizing the two-stage, second order (RK_2); three-stage, third order (RK_3) and four-stage, fourth order (RK_4) explicit Runge–Kutta time integration schemes along with central spatial discretization (CD) schemes of different orders. The optimal time discretization schemes are defined with the help of the correct error propagation Eq. (11). We also compare the performance of the present optimized algorithms with some recently developed optimal time discretization schemes in [1,6,12,15,17] and the classical four-stage, fourth order Runge–Kutta (RK_4) scheme.

The paper is organized in the following manner. In the next section, the optimization problem for obtaining superior time discretization schemes is posed that reduces errors due to dispersion. Various optimal time discretization methods are analyzed in this section. In Section 3, new optimized Runge–Kutta (ORK) schemes are analyzed using the solution of the wave propagation problem along with the results obtained by classical Runge–Kutta and other optimal schemes which have been proposed in the literature [1,6,12,15,17]. In Section 4, results of flow inside a 2D-square LDC for $Re = 1000$ obtained by solving Navier–Stokes equations are used to calibrate the methods for accuracy. Furthermore, to test the efficiency of the time discretization methods, the same problem has been solved for a higher Reynolds number of $Re = 10,000$. This is done with a view to compare the dispersion properties of the schemes, as the flow is unsteady at this Re. We also solve another benchmark propagation problem to report the speed-up of the present ORK methods as compared to RK_4 and another optimal methods.

2. Mathematical formulation of the problem

We consider the general case of a autonomous system of ordinary differential equations of the form

$$\frac{du}{dt} = F(u(t)); \quad t \geqslant t_0 \tag{12}$$

and the initial condition is given by $u(t_0) = u_0$. This analysis is valid for partial differential equation, after the spatial discretization is performed.

The general form of an explicit, pth order s-stages Runge–Kutta method for computing the numerical approximation from u^n to u^{n+1} is

$$\begin{aligned} u^{n+1} &= u^n + \sum_{i=1}^{s} W_i k_i \\ k_i &= \Delta t F\left(u^n + \sum_{j=1}^{i-1} a_{ij} k_j\right). \end{aligned} \tag{13}$$

The parameters a_{ij}'s and the weights W_i's are chosen to make the numerical value u^{n+1} closer to exact value $u(t^{n+1})$ obtained by Taylor series expansion for the scheme in Eq. (13). Matching of the terms determines the order of accuracy and the truncation error. The coefficient must satisfy order conditions obtained by Taylor series expansion of $u(t^{n+1})$. Here, we have considered only the explicit Runge–Kutta schemes for which $p = s$ i.e. the order is also equal to the number of stages. The explicit form of these conditions for different order of accuracy are given as follows.

For the three-stage, third order Runge–Kutta (RK_3) method, the explicit form of the corresponding order conditions are [5,13,16]:

$$\begin{aligned} &W_1 + W_2 + W_3 = 1 \\ &W_2 a_{21} + W_3 (a_{31} + a_{32}) = \frac{1}{2} \\ &W_2 a_{21}^2 + W_3 (a_{31} + a_{32})^2 = \frac{1}{3} \\ &W_3 a_{32} a_{21} = \frac{1}{6}. \end{aligned} \tag{14}$$

One can obtain the corresponding relations for RK_2 scheme from the first two equations in the above by setting, $W_3 = 0 = a_{31} = a_{32}$.

For the four-stage, fourth order Runge–Kutta (RK_4) method, the explicit form of the order conditions are:

$$\begin{aligned}
&W_1 + W_2 + W_3 + W_4 = 1\\
&W_2 a_{21} + W_3 (a_{31} + a_{32}) + W_4 (a_{41} + a_{42} + a_{43}) = \frac{1}{2}\\
&W_2 a_{21}^2 + W_3 (a_{31} + a_{32})^2 + W_4 (a_{41} + a_{42} + a_{43})^2 = \frac{1}{3}\\
&W_3 a_{32} a_{21} + W_4 [a_{21} a_{42} + a_{43} (a_{31} + a_{32})] = \frac{1}{6}\\
&W_2 a_{21}^3 + W_3 (a_{31} + a_{32})^3 + W_4 (a_{41} + a_{42} + a_{43})^3 = \frac{1}{4}\\
&W_3 [a_{32} a_{21}^2 + 2a_{21} a_{32} (a_{31} + a_{32})] + W_4 [a_{42} a_{21}^2 + a_{43} (a_{31} + a_{32})^2\\
&+ 2(a_{41} + a_{42} + a_{43})\{(a_{31} + a_{32}) a_{43} + a_{42} a_{21}\}] = \frac{1}{3}\\
&W_4 a_{43} a_{32} a_{21} = \frac{1}{24}.
\end{aligned} \tag{15}$$

These equations are once again obtained by comparing the Taylor series expansion of $u^{(n+1)}$ and $u(t^{n+1})$. These are also given in [5,13,16], except that we obtain an equation less than those given there. The difference is due to the splitting of the coefficient of h^4 in [5,13,16], as given above in a single relation in the second-last equation of Eq. (15). However, one notices that this does not alter the value of parameters obtained for the classical method.

In the present work, optimization of time advancing explicit Runge–Kutta schemes coupled with spatial discretization is considered to get superior DRP properties of the numerical solution for an autonomous system. This is performed by examining the error in the spectral plane, instead of working with Eqs. (14) and (15). For this purpose, we consider the time evolution equation rewritten as:

$$\frac{\partial u}{\partial t} = F(u). \tag{16}$$

An explicit s-stage Runge–Kutta scheme can be written as [13]:

$$u^{(i)} = u^{(n)} + \Delta t \sum_{j=1}^{i-1} a_{ij} F^{(j)} \tag{17}$$

$$u^{(n+1)} = u^{(n)} + \Delta t \sum_{j=1}^{s} W_j F^{(j)} \tag{18}$$

where the stage number i runs from 1 to s. The above formulation requires a lot of memory because at the ith stage all the $F^{(j)}$'s up to the previous stage need to be stored, as given in (17). The Runge–Kutta scheme can be implemented in a form that requires less storage as given by [27],

$$u^{(i)} = u^{(n)} + \Delta t\, \alpha_i F^{(i-1)} \tag{19}$$

$$u^{(n+1)} = u^{(n)} + \Delta t \sum_{i=1}^{s} W_i F^{(i)}. \tag{20}$$

Present analysis and implementations are based on this low storage form of the methods.

The amplification factor for the Runge –Kutta scheme (for $p = s$) in k-space, can be written for Eq. (1) in the form given in [27],

$$G_{num} = 1 + \sum_{j=1}^{p} (-1)^j a_j A^j. \tag{21}$$

Also for Eq. (1), one can obtain the exact amplification factor [12] as, $G_{exact} = e^{-iN_c kh}$. Eq. (21) is a polynomial approximation of G_{exact} and the coefficients a_j's can be either chosen to minimize the truncation error by taking $a_j = 1/j!$ or by minimizing the error in k-space, as given in Eq. (11). Hu et al. [12] considered the 1D convection equation to minimize the difference between numerical and exact amplification factors. Similarly in [1,15], an optimization was performed by defining the solution error as the L_2-norm of the difference between numerical and exact solutions, given by $|G_{num}^n - e^{-inN_c kh}||u_0|_2$ obtained at $t = n\Delta t$, where $|u_0|_2$ defining the L_2-norm of the initial condition.

In the present work, the coefficient(s) a_j's in Eq. (21) are related to the parameters of the Runge–Kutta method by the analysis in k-space. For RK_2 method, this leads to relations between the α_i's and W_i's for the low storage version in Eqs. (19) and (20) as

$$\begin{aligned}
&W_1 + W_2 = a_1\\
&W_2 \alpha_1 = a_2.
\end{aligned} \tag{22}$$

Similarly, for RK_3 scheme we have the following relations

$$\begin{aligned} &W_1 + W_2 + W_3 = a_1 \\ &W_2\alpha_1 + W_3\alpha_2 = a_2 \\ &W_3\alpha_1\alpha_2 = a_3. \end{aligned} \tag{23}$$

Finally, for the RK_4 scheme we have the following relations

$$\begin{aligned} &W_1 + W_2 + W_3 + W_4 = a_1 \\ &W_2\alpha_1 + W_3\alpha_2 + W_4\alpha_3 = a_2 \\ &W_3\alpha_1\alpha_2 + W_4\alpha_2\alpha_3 = a_3 \\ &W_4\alpha_1\alpha_2\alpha_3 = a_4. \end{aligned} \tag{24}$$

Let us obtain an optimized time discretization strategy that minimizes overall error, including dissipation, phase and dispersion components of the basic scheme in (11). First, we consider the RK_2 scheme coupled with various central difference schemes. In the process, we left the last coefficient free in the expression for G_{num}, i.e. we consider $a_2 = a$ and $a_1 = 1$, so that the method retains first order formal accuracy, while the consistency condition is satisfied. Thus, the amplification factor for Eq. (1) is written as,

$$G_2 = 1 - A + aA^2. \tag{25}$$

It remains to fix the value of a via an optimization process and then using Eq. (22), we obtain the other coefficients of the optimized two-stage, second order Runge–Kutta (ORK_2) scheme. Similarly for the RK_3 method, we leave the last two coefficients in G_{num} as free parameters, so that $a_2 = b$ and $a_3 = a$. Once again, the method is first order accurate only. For the RK_4 method, we set $a_3 = b$, and $a_4 = a$ in (21), so that the resultant optimal method is formally second order accurate. Thus, the amplification factor for Eq. (1), for the optimized ORK_3 and ORK_4 schemes are given respectively by:

$$G_3 = 1 - A + bA^2 - aA^3 \tag{26}$$

$$G_4 = 1 - A + \frac{A^2}{2!} - bA^3 + aA^4. \tag{27}$$

Having obtained a and b by optimization, one can solve (23) and (24) to obtain the optimized Runge–Kutta (ORK) methods. In [12], the following objective function was minimized:

$$F(a,b,N_c) = \int_0^{\gamma} |G_{num} - G_{exact}|^2 \, d(kh) \tag{28}$$

where $\gamma = \alpha\pi$ with α in $[0,1]$. The same objective function is used in the present exercise. However, in addition to minimizing F, we also explicitly constrain the schemes following (11) to ensure neutral stability, minimum phase and dispersion errors through the satisfaction of the following inequalities:

$$F_1(a,b,N_c) = \int_0^{\gamma_1} ||G| - 1| \, d(kh) \leqslant \epsilon_1 \tag{29}$$

$$F_2(a,b,N_c) = \int_0^{\gamma_2} \left| \left(\frac{V_{gN}}{c}\right) - 1 \right| d(kh) \leqslant \epsilon_2 \tag{30}$$

$$F_3(a,b,N_c) = \int_0^{\gamma_3} \left| \left(\frac{c_N}{c}\right) - 1 \right| d(kh) \leqslant \epsilon_3 \tag{31}$$

where γ_i and ϵ_i are constants chosen to satisfy numerical properties of the basic method. Although, we prescribe a small tolerance in ϵ_1, we are interested in looking for numerical parameters which ensure neutral stability for large range of (kh, N_c).

To solve this constrained optimization problem, we have used the grid-search technique [19] to locate the feasible region in (a,b)-plane using the constraints given in (29)–(31) for different, but fixed value of N_c. While a and b are functions of N_c, we would like to obtain fixed values of a and b for the ORK schemes for a particular N_c, but that could be used over a longer range of CFL number. In that sense, these values of a and b will be near-optimal.

For second (CD_2), fourth (CD_4) and sixth order accurate (CD_6) spatial discretization schemes for the first derivative, one can show that $A = iN_c \sin(kh), \frac{iN_c}{3}[4 - cos(kh)]\sin(kh)$ and $\frac{iN_c}{30}[\sin(3kh) - 9\sin(2kh) + 45\sin(kh)]$, respectively. For the results presented here, we have chosen $\gamma = \pi/2$ for the objective function and the tolerances needed in (29)–(31) for the specific methods are as indicated below. These values depend upon the spatial discretization methods, while they do not depend upon the temporal discretization schemes. Thus, we have used the following tolerances for CD_2 spatial discretization schemes: $\epsilon_1 = 10^{-5}$, $\epsilon_2 = 0.01$ and $\epsilon_3 = 0.05$, while the ranges of kh used to satisfy the constraints are given by: $\gamma_1 = 1.0$, $\gamma_2 = 0.4$ and $\gamma_3 = 1.0$. For the CD_4 spatial discretization scheme, the limits on kh are: $\gamma_1 = 1.0$, $\gamma_2 = 1.0$, $\gamma_3 = 1.0$ and the tolerances are: $\epsilon_1 = 10^{-5}$, $\epsilon_2 = 0.01$ and $\epsilon_3 = 0.003$. For the CD_6 spatial discretization scheme, limits are fixed as: $\gamma_1 = 1.0$, $\gamma_2 = 1.0$, $\gamma_3 = 1.0$; while the tolerances are fixed by: $\epsilon_1 = 10^{-5}$; $\epsilon_2 = 0.01$ and

$\epsilon_3 = 0.007$. It is noted that the constraints given by (29)–(31) makes the search for optimum value difficult for lower order methods, for which ϵ_i's have to be relatively higher.

2.1. Optimization of RK_2 scheme coupled to CD_2, CD_4 and CD_6 schemes

Here, we have optimized RK_2 scheme, coupled to CD_2, CD_4 and CD_6 schemes for solving Eq. (1). For this optimized scheme, values of a as a function of N_c are shown in Fig. 1a for the three spatial discretization schemes. For the original scheme, $a = 1/2$, and is indicated by the dash-dotted lines in the sub-figures. For very low values of N_c, optimal values of a lie close to 1/2 as in the classical method. For larger N_c, the value of a changes from the classical value by a very small amount.

Having fixed the value of $a_1 = 1$, one can solve Eq. (22), to fix W_1, W_2 and a_{21}. This leaves one degree of freedom to choose any one of the unknowns. We have taken $W_1 = 0$, so that $W_2 = 1$ and $a_{21} = a$. This choice of W_1 helps one reduce the number of operations in implementing the ORK_2 scheme which is given by,

$$u^{(1)} = u^{(n)} + a\,\Delta t\,F\left[u^{(n)}\right] \tag{32}$$

$$u^{(n+1)} = u^{(n)} + \Delta t\,F\left[u^{(1)}\right]. \tag{33}$$

2.2. Optimization of RK_3 scheme coupled to CD_2, CD_4 and CD_6 schemes

Here, we optimize the classical RK_3 scheme coupled to CD_2, CD_4 and CD_6 schemes for Eq. (1). From the basic RK_3 scheme we obtain a and b that retains the first order accuracy of time discretization, while minimizing the objective function given by (28), subject to the constraints in (29)–(31). Results are shown in Fig. 1b, for the three spatial discretization schemes. Values of a and b used in the classical method are shown by dash-dotted lines. We note that a varies significantly from the classical value, while b remains closer to the value in RK_3 scheme. This figure shows that a remains constant for $N_c > 0.25$, irrespective of the spatial discretization scheme. The value of a changes for small values of N_c.

For the optimized ORK_3 scheme, we fix the values of a and b (with respect to N_c) as discussed above. Three equations in (23) are for five unknowns, allowing one to fix any two of them. Here, we have taken $W_1 = 0$ and $W_2 = 0$ to reduce the number of operations in the implementation of the ORK_3 algorithm. This fixes: $W_3 = 1$, $\alpha_2 = b$ and $\alpha_1 = a/b$. The optimal ORK_3 scheme used here is given by,

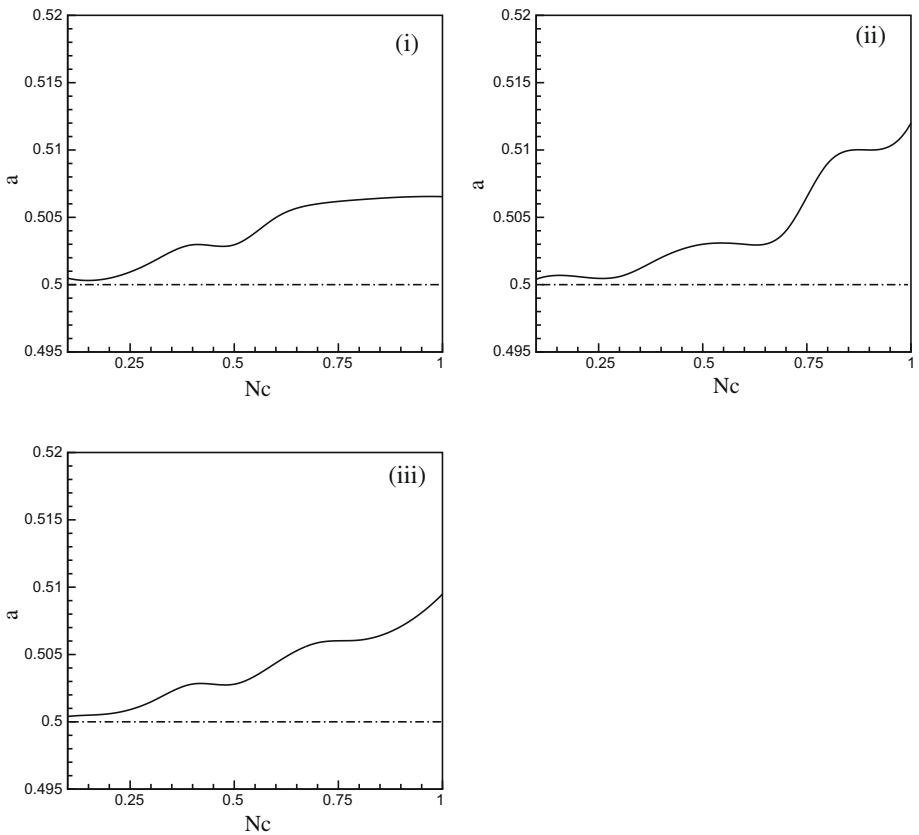

Fig. 1a. Variation of a in Eq. (31), with N_c for (i) $ORK_2 - CD_2$; (ii) $ORK_2 - CD_4$ and (iii) $ORK_4 - CD_6$ schemes.

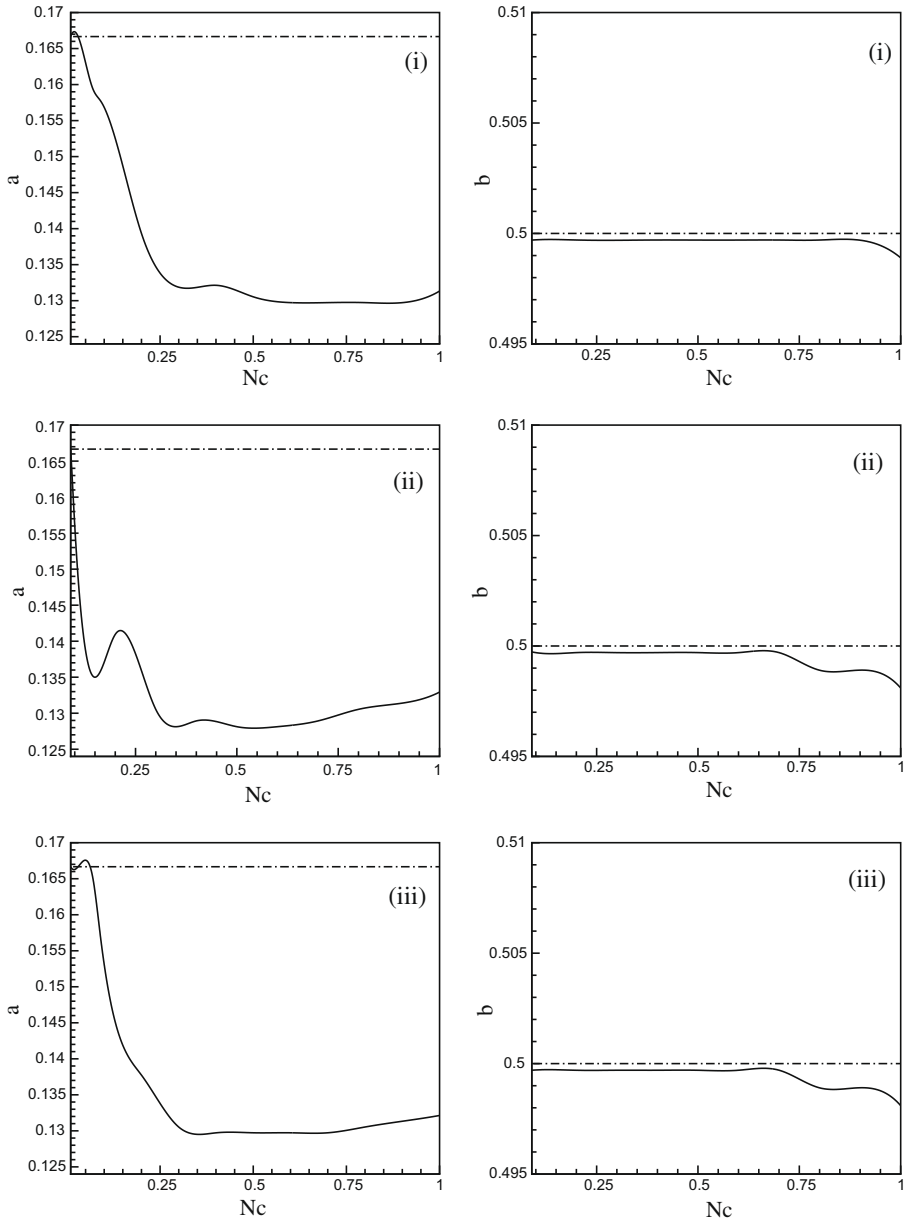

Fig. 1b. Variation of a and b in Eq. (32), with N_c for (i) $ORK_3 - CD_2$; (ii) $ORK_3 - CD_4$ and (iii) $ORK_3 - CD_6$ schemes.

$$u^{(1)} = u^{(n)} + (a/b)\,\Delta t\, F[u^{(n)}] \tag{34}$$

$$u^{(2)} = u^{(n)} + b\,\Delta t\, F[u^{(1)}] \tag{35}$$

$$u^{(n+1)} = u^{(n)} + \Delta t\, F[u^{(2)}]. \tag{36}$$

We would like to emphasize that the different choices of W_1 and W_2 do not alter the numerical properties of the resultant scheme, as the expressions of G_{num} for the schemes remain invariant for different choices of W_1 and W_2 for the ORK_3 scheme, when a and b is kept unchanged. This is also the case for the ORK_2 scheme reported above and the ORK_4 scheme that is reported next.

2.3. Optimization of RK_4 scheme coupled to CD_2, CD_4 and CD_6 schemes

Next, the RK_4 method is optimized when CD_2, CD_4 and CD_6 methods are used for spatial discretization. The resulting second order method provides values of a and b, are as shown versus N_c in Fig. 1c. In this case, both a and b change significantly

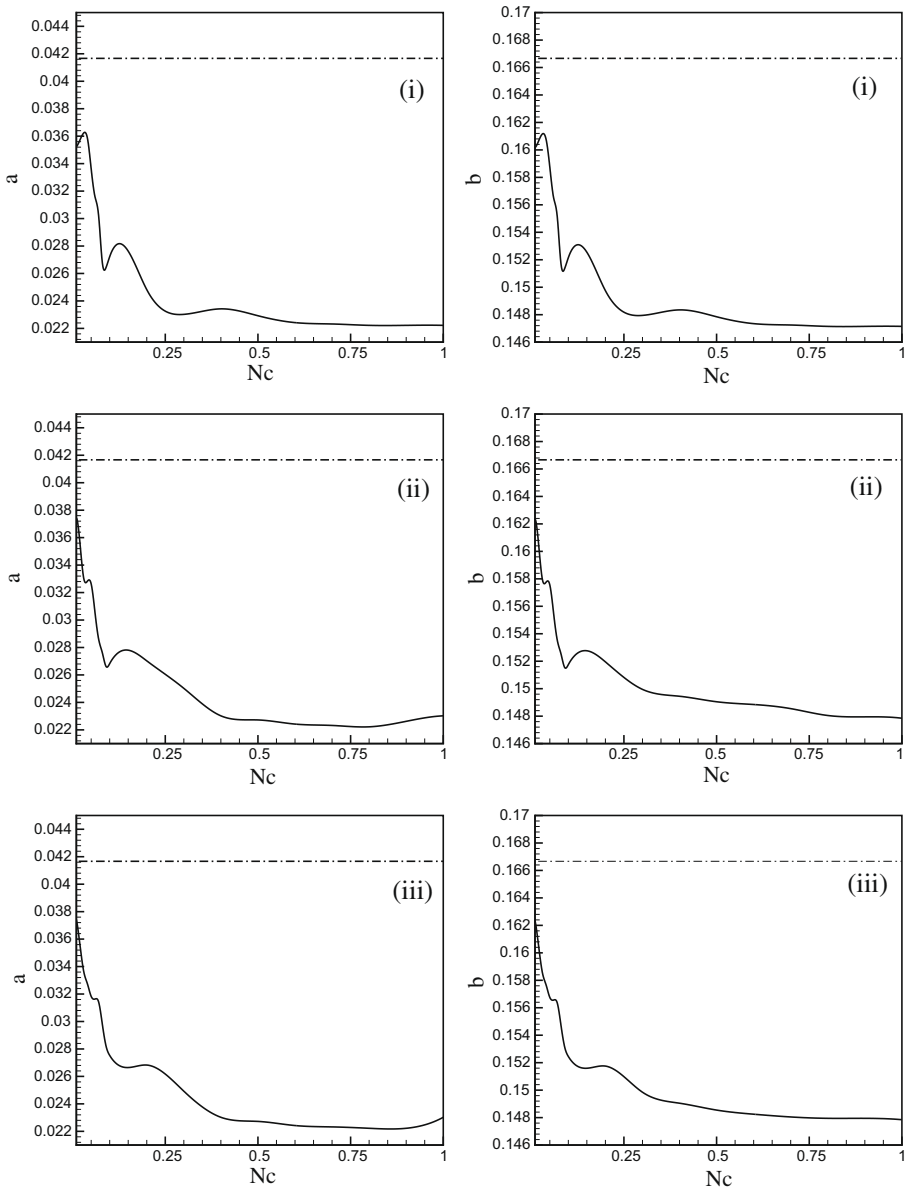

Fig. 1c. Variation of a and b in Eq. (33) with N_c for (i) $ORK_4 - CD_2$; (ii) $ORK_4 - CD_4$ and (iii) $ORK_4 - CD_6$ schemes.

from the values used in the classical scheme. However, the values of a and b remain almost similar for higher values of N_c, and also when one spatial discretization scheme is replaced by another.

To obtain the ORK_4 scheme from the order relations in (24), we note that we have four equations for the seven unknowns. Once again, we will freeze the coefficients a and b with respect to variations in N_c. We have chosen the weights for the ORK_4 scheme to be the same as that is used in the classical RK_4 scheme [13,16] i.e., $W_1 = 1/6;\ W_2 = 1/3$ and $W_3 = 1/3$. This fixes the remaining unknowns as: $W_4 = 1/6;\ \alpha_2 = e/4;\ \alpha_3 = (12\,b/e) - \sqrt{(12\,b/e)^2 - (48\,a/e)}$ and $\alpha_1 = 3/2 - \alpha_2 - \alpha_3/2$, where, $e = 3 - \sqrt{9 - 48\,b}$.

The algorithm for the ORK_4 scheme is given by:

$$u^{(1)} = u^{(n)} + \alpha_1 \Delta t F\left[u^{(n)}\right] \tag{37}$$

$$u^{(2)} = u^{(n)} + \alpha_2 \Delta t F\left[u^{(1)}\right] \tag{38}$$

$$u^{(3)} = u^{(n)} + \alpha_3 \Delta t F\left[u^{(2)}\right] \tag{39}$$

$$u^{(n+1)} = u^{(n)} + \frac{\Delta t}{6}\left[F\left[u^{(n)}\right] + 2F[u^{(1)}] + 2F\left[u^{(2)}\right] + F\left[u^{(3)}\right]\right]. \tag{40}$$

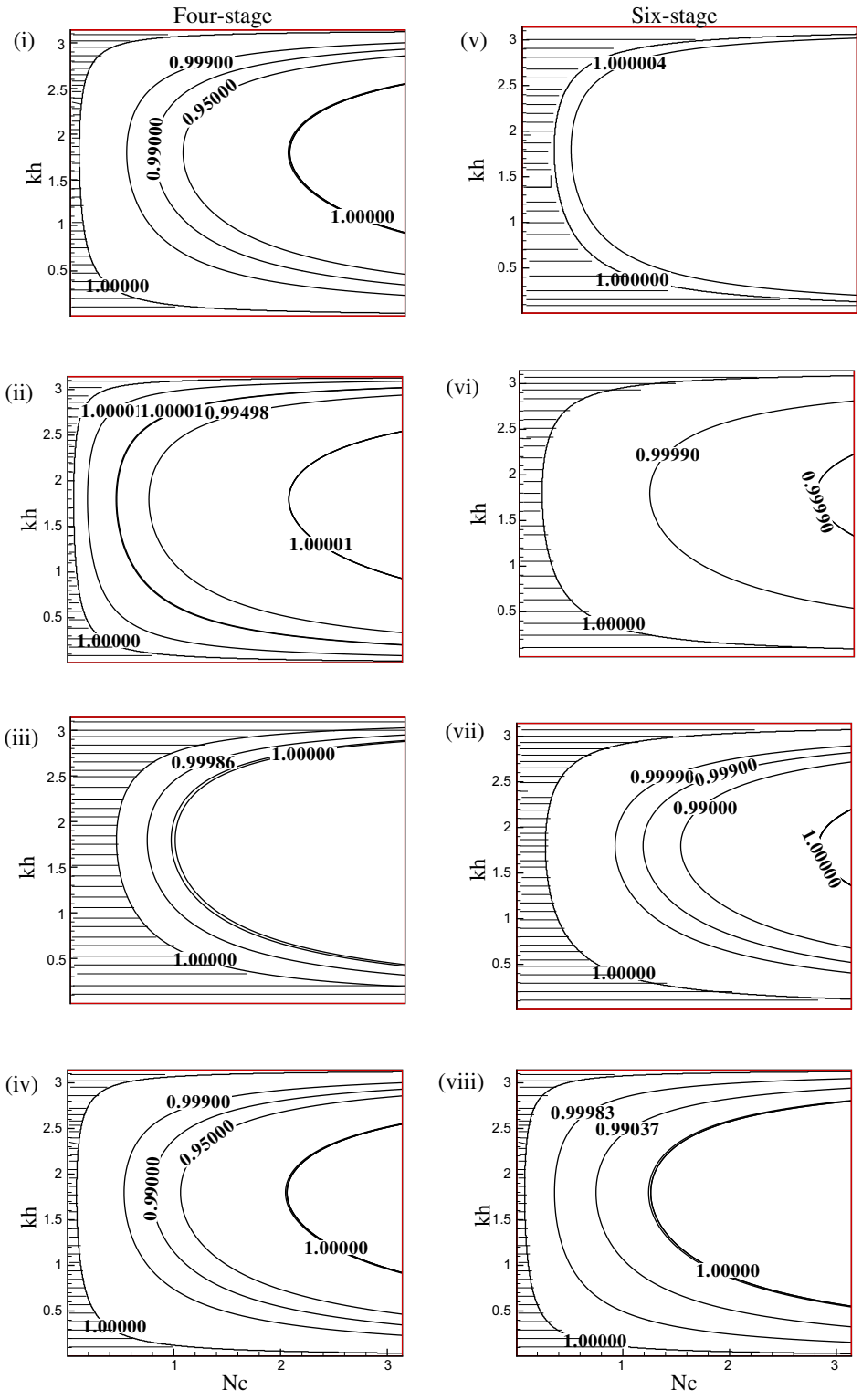

Fig. 2a. Contour plots showing numerical amplification factor ($|G|$) in (kh, N_c)-plane with the CD_4 spatial discretization scheme: (i) RK_4; (ii) LDDRK [3]; (iii) ORK_4; (iv) $ORK24-6$ [1,15]; (v) RK_6; (vi) $LDD46$ [6]; (vii) $ORK46-6$ [1,15] and (viii) six-stage optimized RK scheme [17].

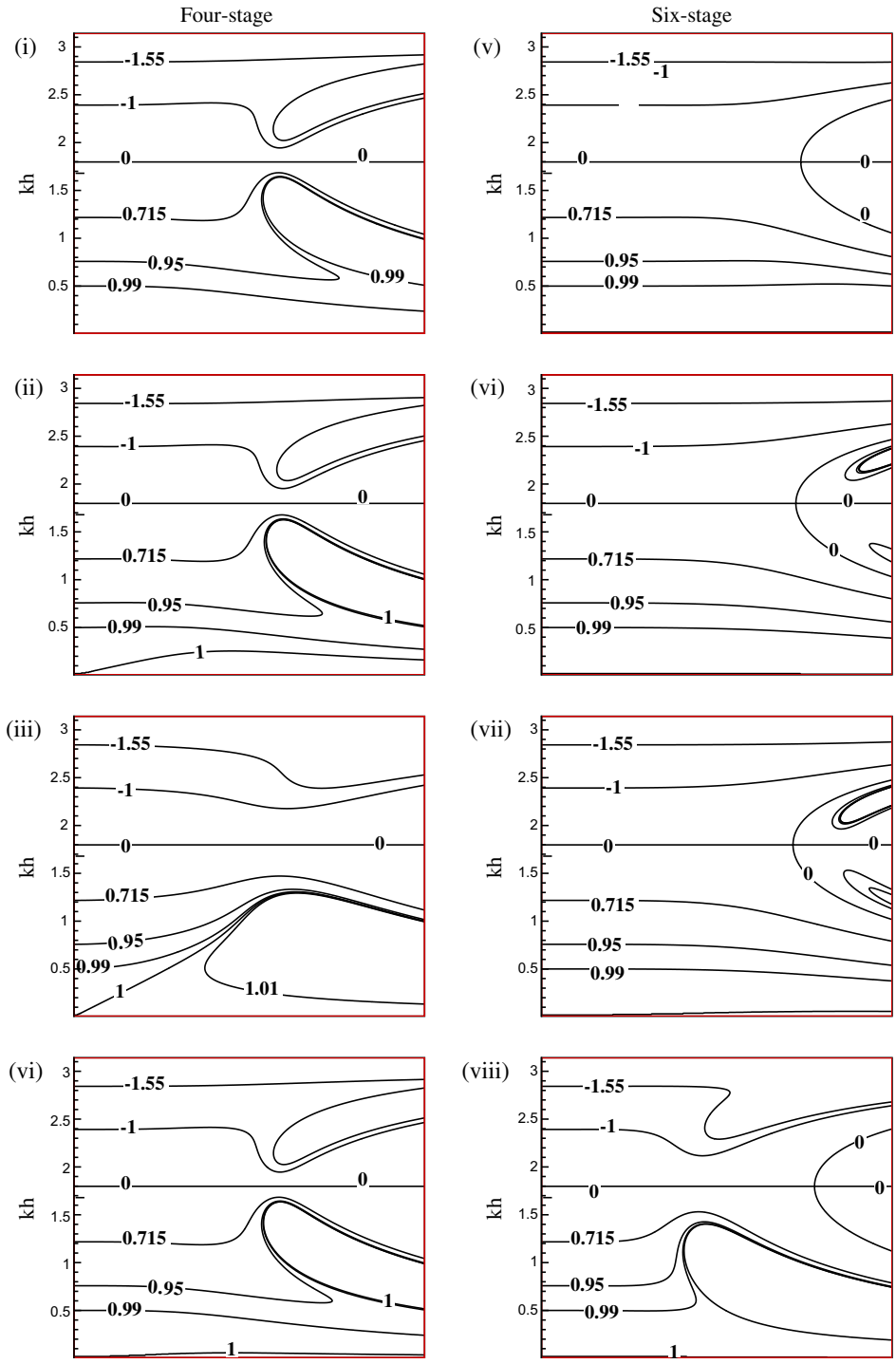

Fig. 2b. Contour plots showing scaled numerical group velocity (V_{gN}/c) in (kh, N_c)-plane with the CD_4 spatial discretization scheme: (i) RK_4; (ii) LDDRK [3]; (iii) ORK_4; (iv) $ORK24-6$ [1,15]; (v) RK_6; (vi) $LDD46$ [6]; (vii) $ORK46-6$ [1,15] and (viii) six-stage optimized RK scheme [17].

2.4. Numerical properties of some specific combinations of temporal and spatial schemes

Having obtained the values of a and b for different combinations of spatial and temporal schemes, we present results for only a few representative combinations as described below. Only the properties of higher order spatial discretization

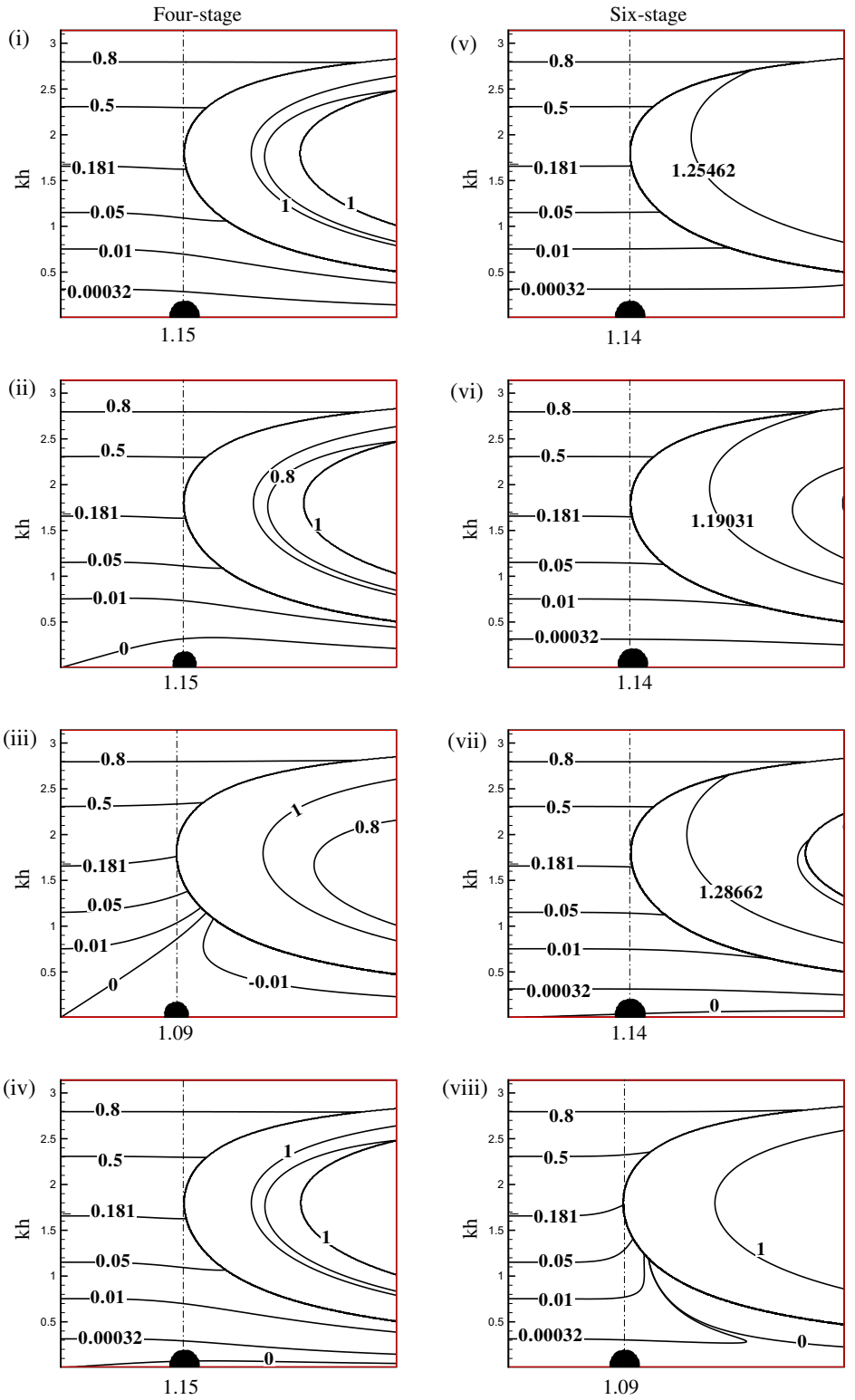

Fig. 2c. Contour plots showing $(1 - c_N/c)$ in (kh, N_c)-plane with the CD_4 spatial discretization scheme: (i) RK_4; (ii) LDDRK [3]; (iii) ORK_4; (iv) $ORK24 - 6$ [1,15]; (v) RK_6; (vi) $LDD46$ [6]; (vii) $ORK46 - 6$ [1,15] and (viii) six-stage optimized RK scheme [17].

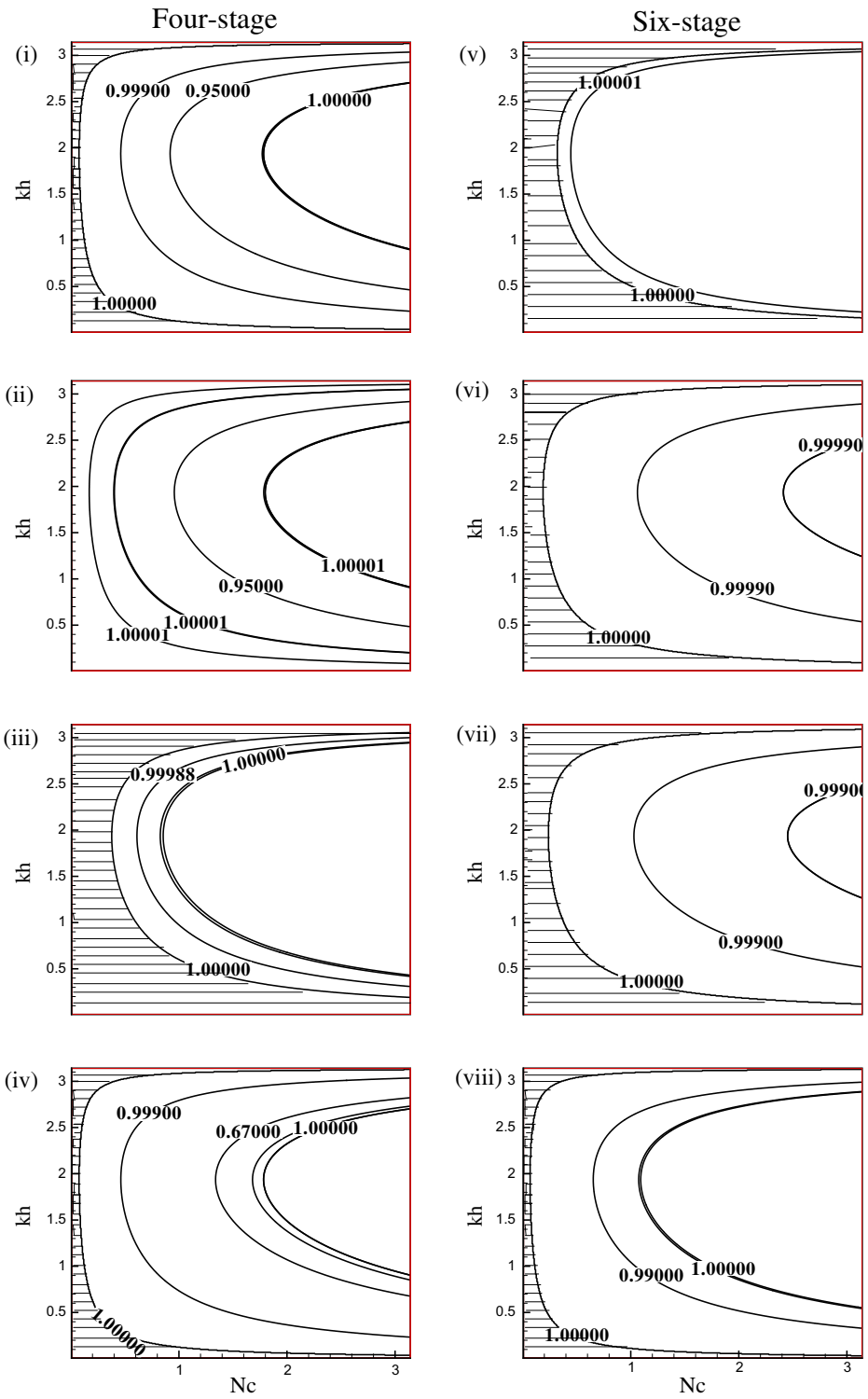

Fig. 3a. Contour plots showing numerical amplification factor ($|G|$) in (kh, N_c)-plane with the CD_6 spatial discretization scheme: (i) RK_4; (ii) LDDRK [3]; (iii) ORK_4; (iv) $ORK24-6$ [1,15]; (v) RK_6; (vi) $LDD46$ [6]; (vii) $ORK46-6$ [1,15] and (viii) six-stage optimized RK scheme [17].

schemes are discussed. First, we show results for the CD_4 spatial discretization method in Fig. 2a–2c. Results are compared for the classical RK_4 and six-stage – sixth order RK_6 schemes along with the optimum schemes of [1,6,12,15,17] and ORK_4 scheme. For the present optimal scheme, we freeze the values of a and b to values obtained for $N_c = 1$.

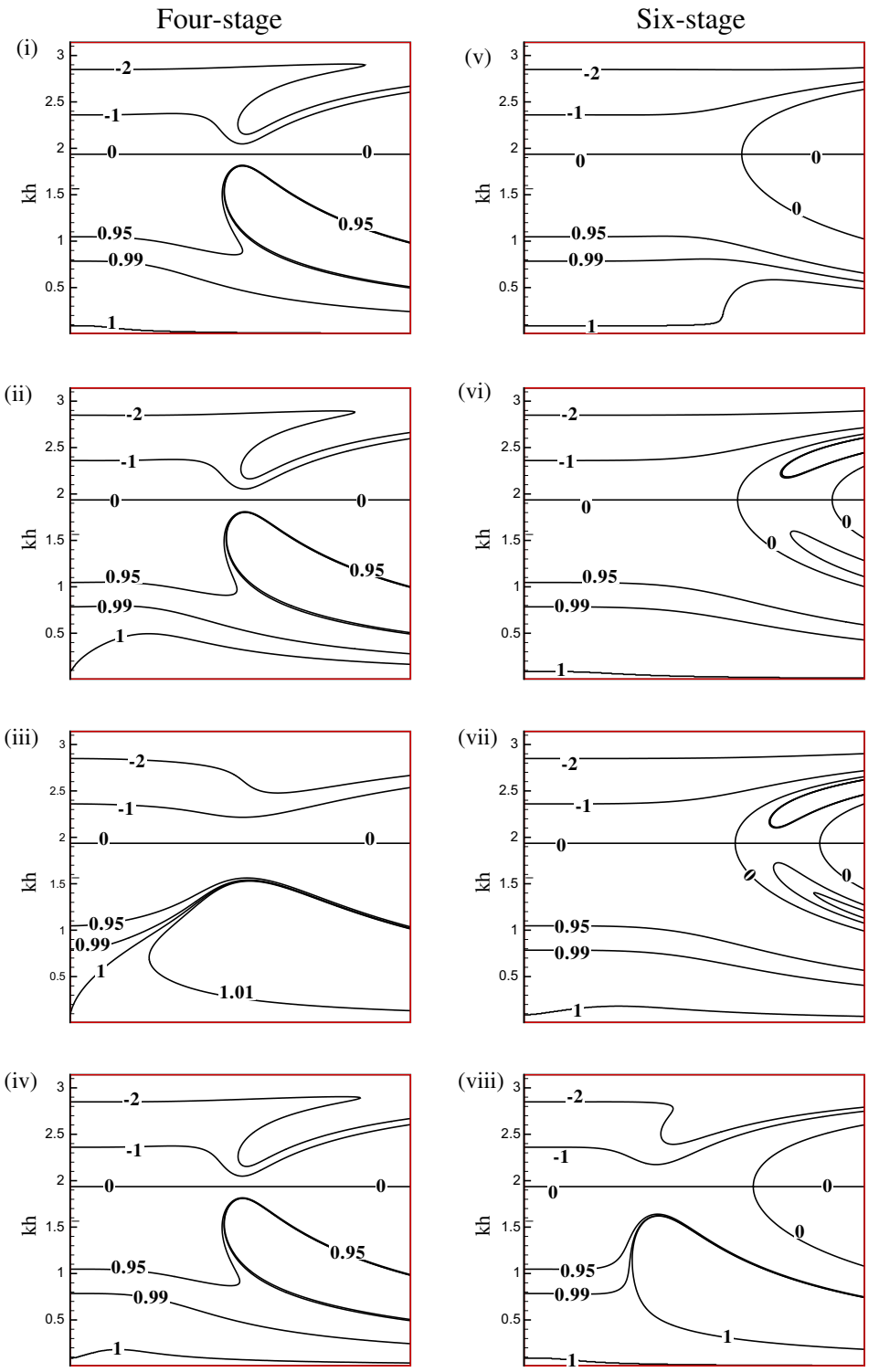

Fig. 3b. Contour plots showing scaled numerical group velocity (V_{gN}/c) in (kh, N_c)-plane with the CD_6 spatial discretization scheme: (i) RK_4; (ii) LDDRK [3]; (iii) ORK_4; (iv) $ORK24-6$ [1,15]; (v) RK_6; (vi) $LDD46$ [6]; (vii) $ORK46-6$ [1,15] and (viii) six-stage optimized RK scheme [17].

In Fig. 2a, numerical amplification factor for an interior node is shown for one-dimensional convection equation where CD_4 discretization scheme is used for space and time discretization is by various indicated methods in the figure. In the sub-figures, regions are marked by horizontal hatched lines representing neutral stability. It is seen that between the two

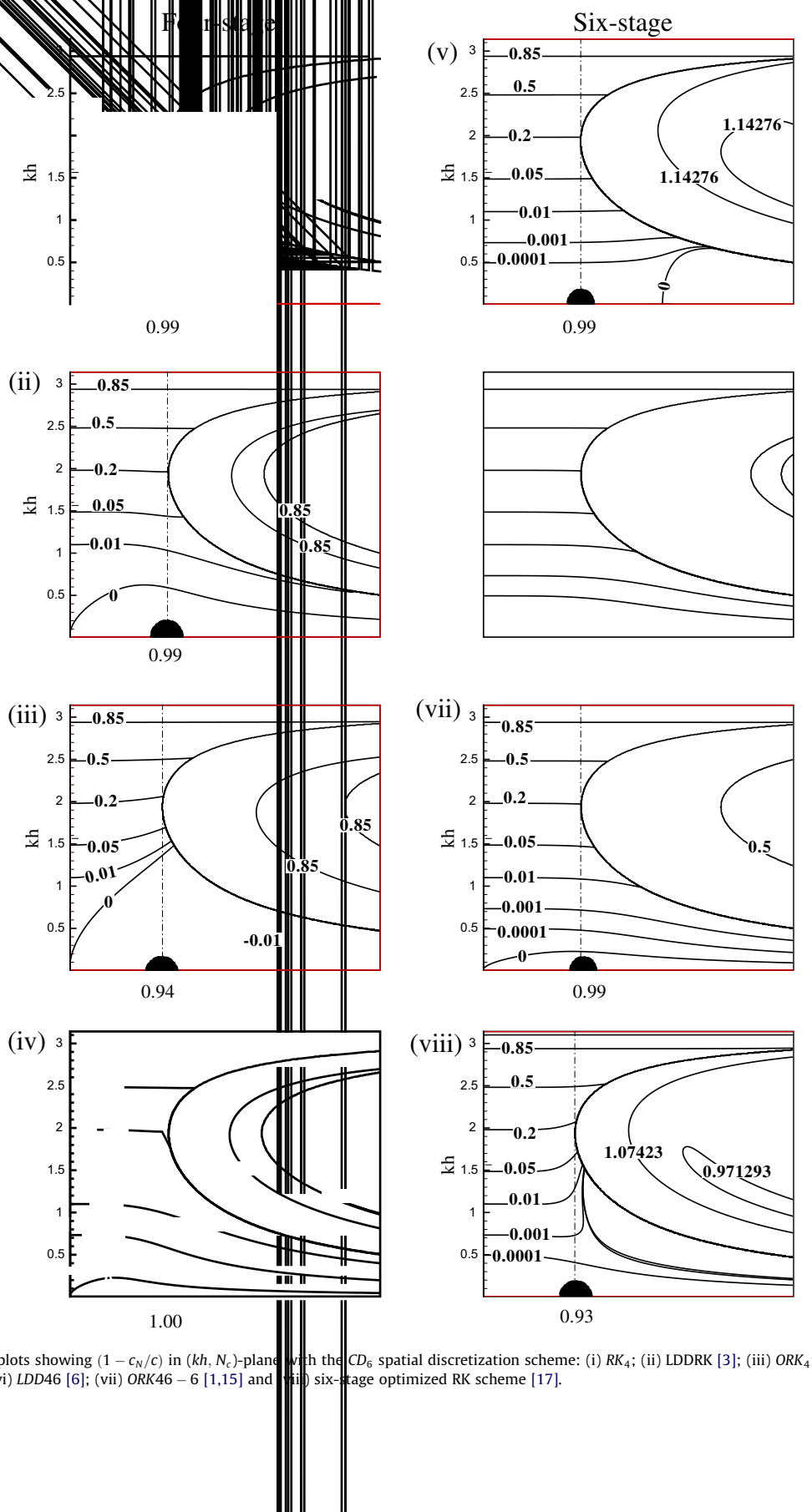

Fig. 3c. Contour plots showing $(1 - c_N/c)$ in (kh, N_c)-plane with the CD_6 spatial discretization scheme: (i) RK_4; (ii) LDDRK [3]; (iii) ORK_4; (iv) $ORK24 - 6$ [1,15]; (v) RK_6; (vi) $LDD46$ [6]; (vii) $ORK46 - 6$ [1,15] and (viii) six-stage optimized RK scheme [17].

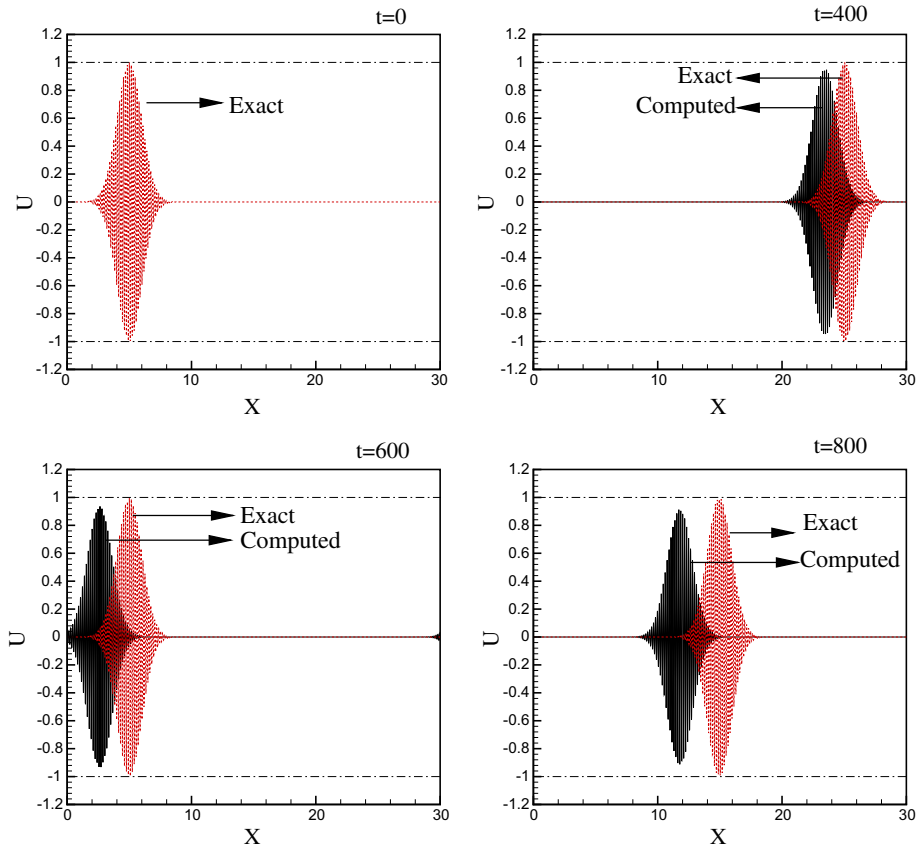

Fig. 4a. Propagation of a computed wave-packet using $RK_4 - CD_2$ scheme with $k_0h = 0.40$ and $N_c = 0.97$ shown by solid line and compared with exact solution (dotted line).

classical schemes, RK_6 is superior to RK_4 scheme. The optimal scheme of [6] belongs to six-stage, fourth order accuracy – with reduced order allowing for an optimal scheme that displays neutrally stable zone similar to RK_6 scheme. However, there is no region of instability for this optimal scheme, unlike the RK_6 scheme. In frame (iv) of Fig. 2a, the $|G|$ – contours of an optimal four-stage, second order scheme due to [1,15] are shown that has similarity with the classical RK_4 and the optimal scheme of [12]. When a six-stage, second order optimal scheme was considered [1,15], one notices significant improvement over RK_6 scheme and the one in [6] – as noted from frames (vi) and (vii) of Fig. 2a. The optimal scheme of [17] is also a basic six-stage method, but the $|G|$-contours shown in frame (viii) show very little improvement even over the classical RK_4 scheme shown in frame (i). Developed optimal ORK_4 scheme in frame (iii) shows the best performance in terms of neutral stability region. This is despite the fact that this is only a four-stage, second order optimal scheme. We note that there are combinations of kh and N_c for which ORK_4 method will be operational, while no other methods would work in terms of numerical neutral stability.

In Fig. 2b, V_{gN}/c contours for the same methods are compared in (kh, N_c)-plane as also shown in Fig. 2a. The classical RK_6 method is slightly better than the RK_4 method in terms of the DRP property. Spurious upstream propagation of waves at high kh occurs for the same value for these two classical methods. The methods due to [1,6,15] also show similar dispersion properties. The four- and six-stage methods of [1,15] show identical dispersion property. Only ORK_4 and the method of [12] show improved dispersion properties for a region close to the origin in (kh, N_c)-plane.

In Fig. 2c, non-dimensional phase error term $(1 - c_N/c)$ is shown in (kh, N_c)-plane for the same methods. The method of [12] and the ORK_4 scheme show lower error as compared to all the other methods, for small values of kh and N_c. Also, one notices a critical value of N_c, above which there is discontinuous increase in phase error for all the methods, with the critical value of N_c marked in the frames. This value is more or less same for all the methods, with ORK_4 and that due to [17] having a lower limit.

In Fig. 3a–3c, results are shown for the CD_6 spatial scheme, used along with same time discretization methods. In Fig. 3a, $|G|$ contours are shown for these methods in (kh, N_c)-plane. It is interesting to note that there is hardly any difference from the corresponding results shown for the CD_4 spatial scheme. This observation is true except for the optimized scheme of [12], for which the neutral stability region completely disappears. For the ORK_4 scheme, a negligible reduction in the value of N_c is noted, up to which one achieves neutral stability.

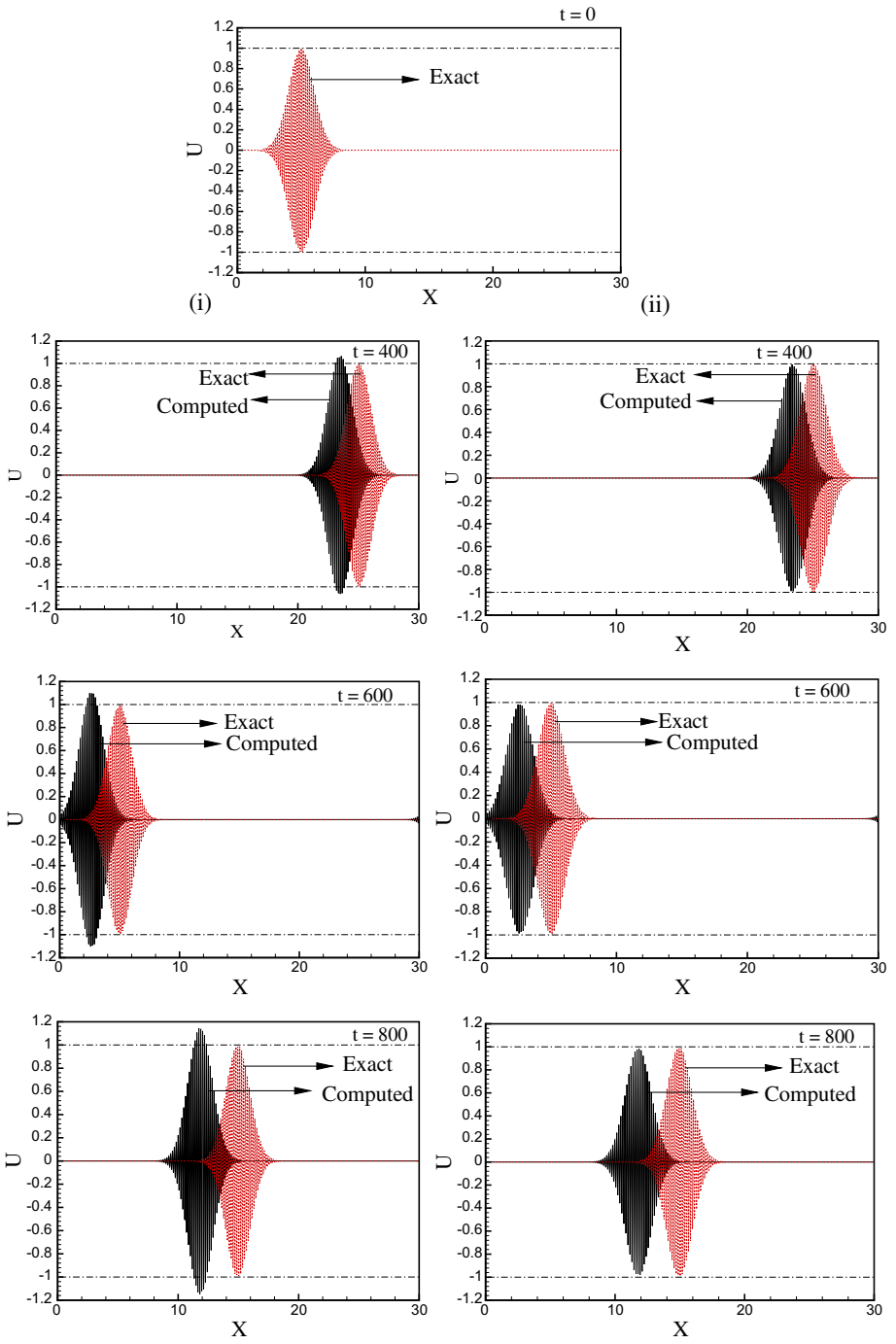

Fig. 4b. Propagation of a computed wave-packet with $k_0h = 0.40$ and $N_c = 0.97$ using: (i) LDDRK (four-stage) [3] – CD_2 scheme and (ii) LDDRK (two-step alternating $RK4-6$) [3] – CD_2 scheme. Computed solution (solid line) compared with exact solution (dotted line).

However, using higher order spatial discretization schemes improves numerical dispersion and phase error properties. In Fig. 3b, the dispersion properties of same time integration schemes are compared with the following changes noted: (i) The critical value above which the numerical solution travels upstream due to spurious dispersion, increases marginally from $kh = 1.8$ to $kh = 1.93$; (ii) the region of $\pm 1\%$ tolerance in the value of V_{gN}/c improves significantly for all the methods. However, the best improvement is seen for the present scheme and that due to [12]. It is noted that the improvement in dispersion property must be the main reason for adopting higher order accurate spatial schemes. Similar improvements are noted also in the phase error property, as shown in Fig. 3c. However, the critical value of N_c, above which phase jumps abruptly is

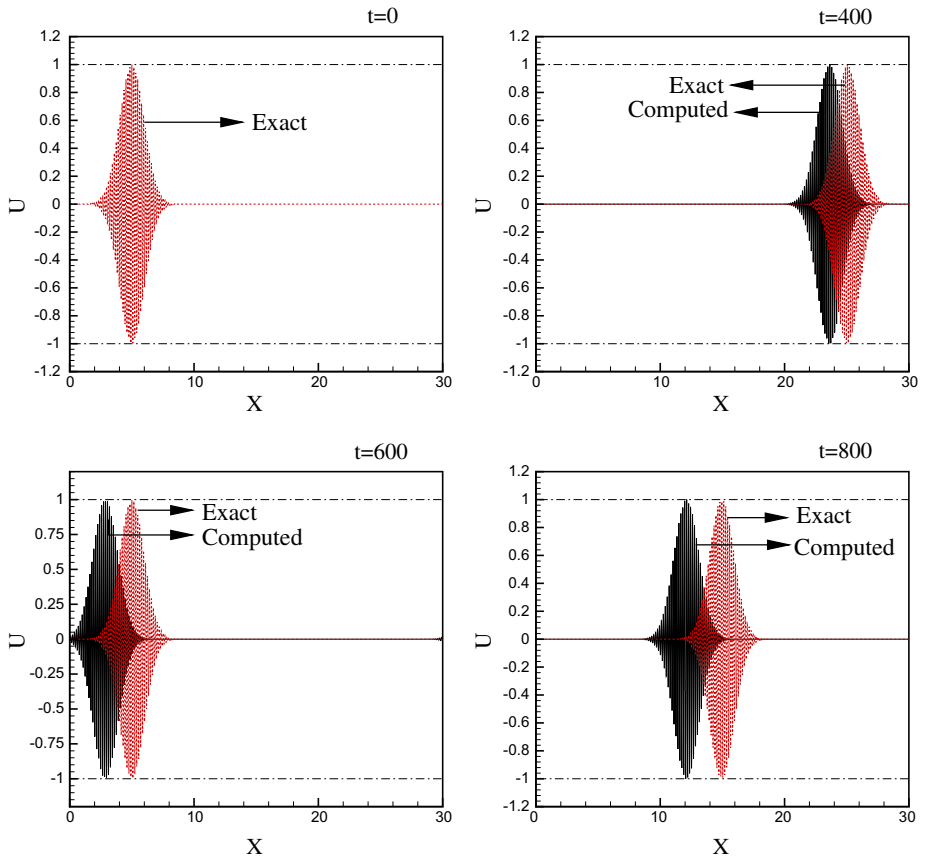

Fig. 4c. Propagation of a computed wave-packet using $ORK_4 - CD_2$ scheme with $k_0h = 0.40$ and $N_c = 0.97$ shown by solid line and compared with exact solution (dotted line).

lowered, by about 15%. In Eq. (11), we noted that the first term on the right hand side affects the error evolution via this $(1 - c_N/c)$ term. This contribution will be significant for solution with sharp gradients (as it depends upon $\frac{\partial u_N}{\partial x}$ also). Figs. 2a–2c and 3a–3c indicate the effects of dispersion error that can not be simply eliminated or reduced by grid refinement alone.

3. Solving wave propagation problem

Numerical properties of Figs. 1a–1c, 2a–2c, 3a–3c determine the levels of error and further careful tests are conducted to highlight these by solving Eq. (1). The optimization performed here and also in [1,6,12,15,17], are made based on this equation as the objective function. However, in the present effort the optimization process is taken further by treating it as a constrained optimization problem, with the constraints minimizing errors identified in (11). To test for errors contributed by $|G| \neq 1$, we have considered propagation of a wave-packet, as shown in Fig. 4a–4c. The wave-packet is given by, $u(x) = e^{-0.5(x-5)^2}\cos[k_0(x-5)]$ and in the present exercise, a domain $0 \leqslant x \leqslant 30$ with constant grid spacing ($h = 0.01$), is used for all reported computations. The problem has been treated here as being periodic in the domain, with the wave-packet defined by $k_0h = 0.40$, and solution obtained by four time integration schemes for $N_c = 0.97$. In Fig. 4a, computed results obtained with CD_2 spatial scheme and classical RK_4 time integration method are compared with exact solution, at the indicated time instants. From the solution at $t = 400$ one notes mild attenuation of the signal, as well as dispersion error. Such errors increase with time, as noted from the snapshots at $t = 600$ and 800. In Fig. 4b, similar comparison is shown between the exact and the numerical solution obtained using the methods of [12] for time discretization along with CD_2 spatial discretization. In Fig. 4b(i), numerical results obtained by the four-stage optimized method due to [12] are displayed. Here, results show slightly lower dispersion error, as compared to the results of Fig. 4a. Also, instead of attenuation of signal, one notices mild amplification – that is consistent with the trend shown for the $|G|$ contours in Fig. 2a and 3a for this time discretization method when used with CD_4 and CD_6 spatial discretizations, respectively. In [12], the authors also have suggested using time integration by a *two-step alternating* method, in which during the first step classical RK_4 scheme is used that is followed by an optimized six-stage, second order Runge–Kutta method. These results are shown in Fig. 4b(ii). While the opti-

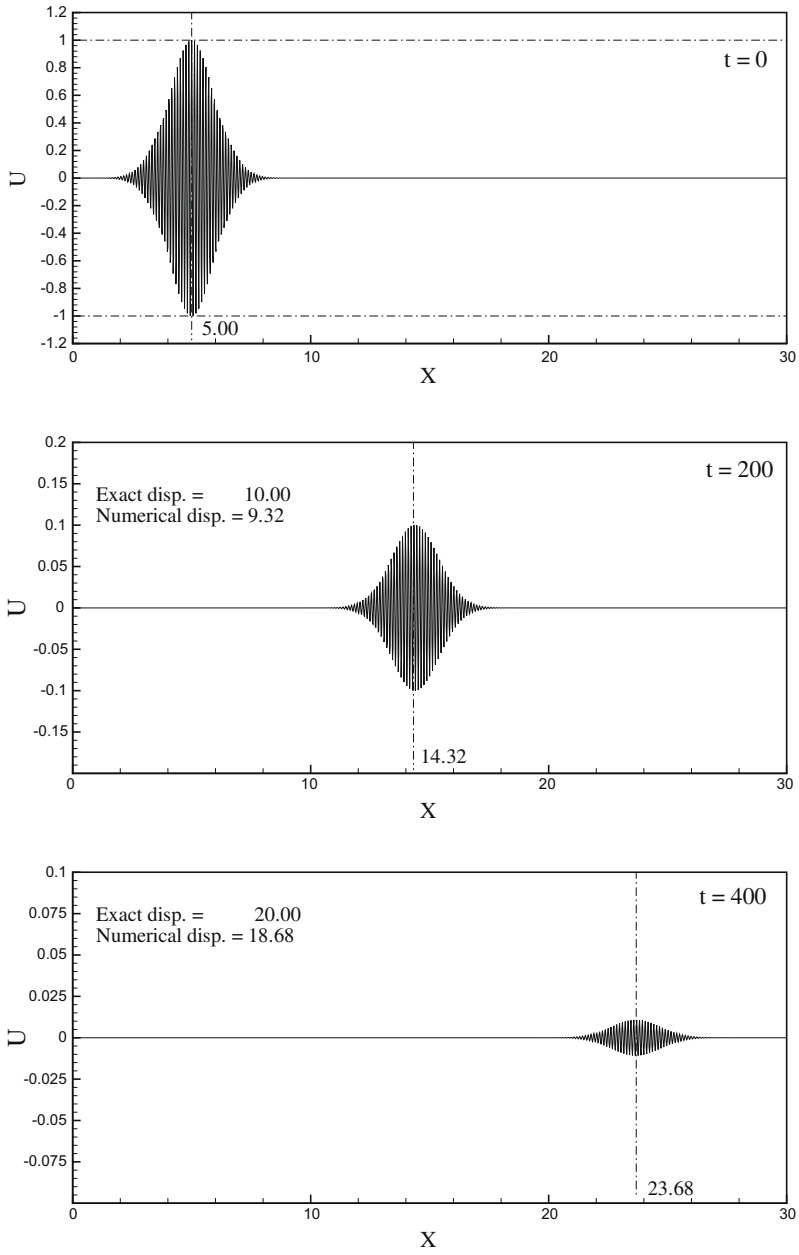

Fig. 5a. Propagation of a computed wave-packet using $RK_4 - CD_6$ scheme with $k_0h = 1.0562$ and $N_c = 0.8904$. Vertical dash-dotted line indicates the location of the center of the computed packet.

mized four-stage method was found to be mildly unstable, the *two-step alternating method* produced results those are found to be mildly attenuated. Thus, it appears that the improvement is brought about by significant increase in additional two-stages of computations.

In Fig. 4c, the exact solution is compared with the numerical results obtained using the present optimal ORK_4 time integration scheme with CD_2 scheme for spatial discretization. While one notices almost similar dispersion error as compared to the method of [12], a distinct improvement is seen for the amplitude envelope that does not amplify or attenuate, even at $t = 800$.

Another test has been performed to study the dispersion and dissipation error for the propagation of the same packet, for which results are shown in Fig. 5a–5c. In this case with CD_6 spatial discretization scheme, the numerical parameters, $N_c = 0.8904$ and $k_0h = 1.0562$ have been chosen to explain certain properties shown in Fig. 3a–3c, for the same four time integration schemes used in Fig. 4. In Fig. 5a, numerical results are shown for $RK_4 - CD_6$ method that display larger amount

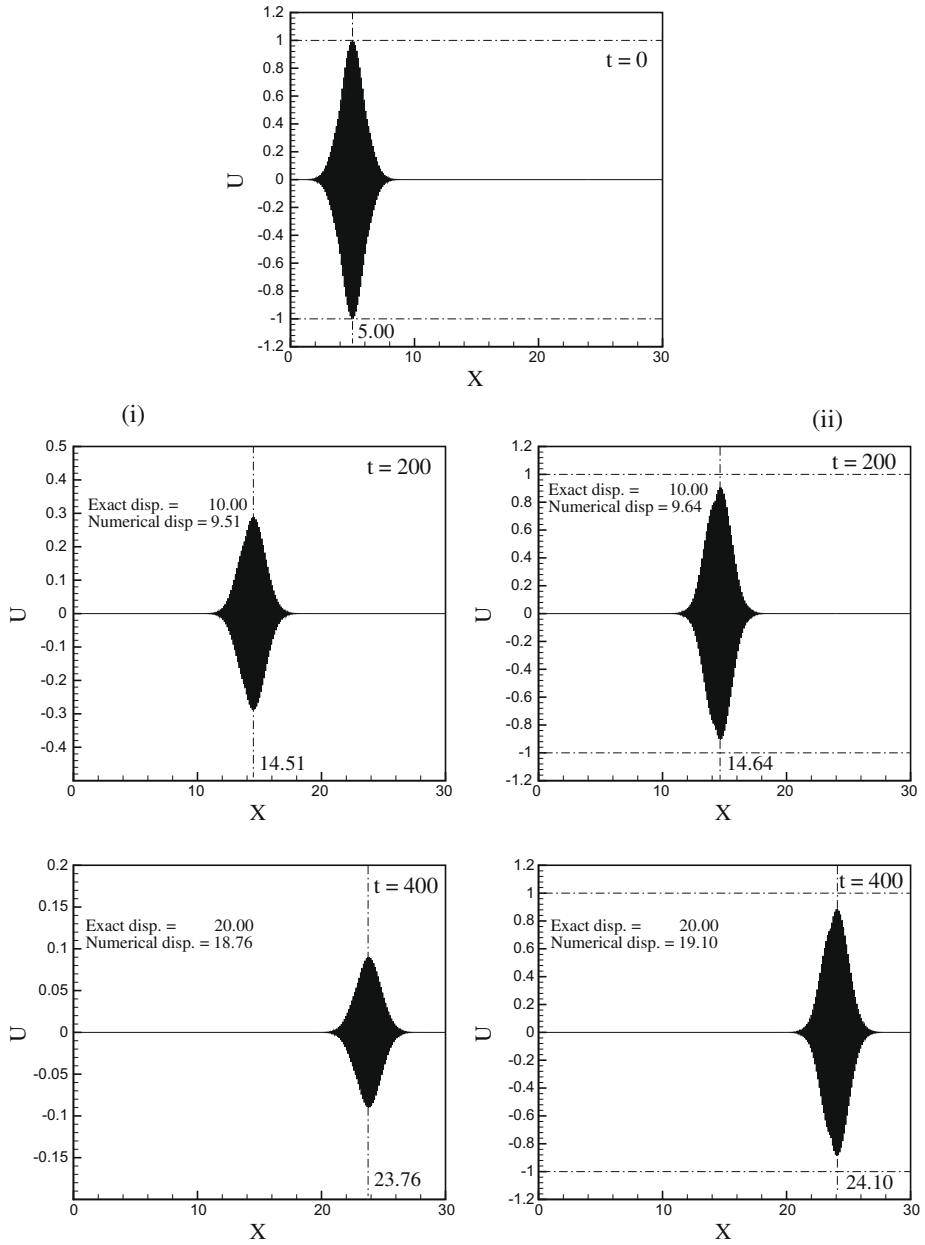

Fig. 5b. Propagation of a computed wave-packet with $k_0h = 1.0562$ and $N_c = 0.8904$ using: (i) LDDRK (four-stage) [3] $-CD_6$ scheme and (ii) LDDRK (two-step alternating $RK4-6$) [3] $-CD_6$ scheme. Vertical dash-dotted line indicates the location of the center of the computed packet.

of dissipation as compared to the classical $RK_4 - CD_2$ scheme of Fig. 4a. At $t = 400$, the signal amplitude comes down to less than 0.025, starting from an initial unit amplitude. One can also note a slightly reduced dispersion error (comparing the exact location of the center of the packet in the figure by a vertical dash-dotted line with the numerical location), as compared to that in Fig. 4a. This behavior follows the contour values shown in Fig. 3a–3c. In Fig. 5b(i), numerical solution obtained by the optimized four-stage method of [12] are displayed. In Fig. 5b(ii), results are shown for the *two-step alternating* method as described for the results of Fig. 4b(ii). As noted in Fig. 4b(ii), here also one notices attenuation of the wave-packet. Also, the dispersion is lesser in this case. Numerical results shown in Fig. 5c obtained by ORK_4 method, shows significantly less attenuation, while the solution does not show any dispersion. The choice of the numerical parameters for Figs. 4 and 5 were made to highlight specifically the comparative aspects of dissipation and dispersion.

Finally to test error due to phase mismatch given by $(1 - c_N/c)$, we have considered the propagation of a pulse with trapezoidal form, as marked in Fig. 6a by *ABCD*, at $t = 0$. The slant angles have been taken as 0.45π and 0.55π at *A* and *D*, respectively. Such discontinuities in slope give rise to Gibbs' phenomenon [21]. We have chosen the values of $N_c = 0.9400$ and

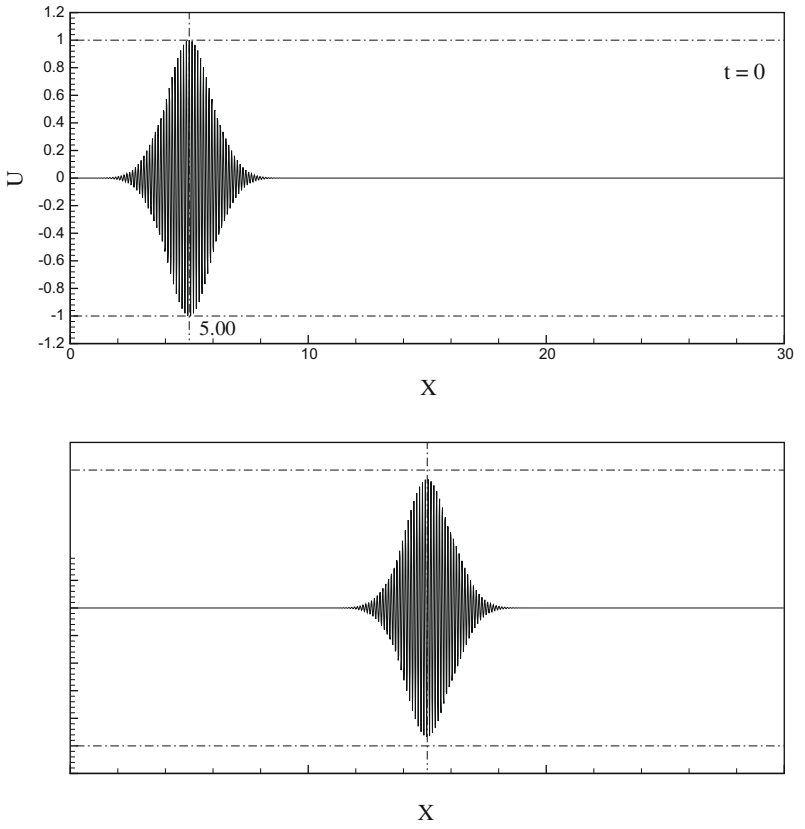

$k_0h = 1.3660$ to highlight the Gibbs' phenomenon triggered by phase error, displayed by three time integration methods. The solution of (1) with this initial condition has been performed for a time up to $t = 900$. Displayed results in Fig. 6a show upstream propagation of spurious oscillations caused by phase and dispersion errors via Gibbs' phenomenon. Reason behind the Gibbs' phenomenon and a method to suppress spurious oscillations is reported in [21]. For classical RK_4 method, one notices small upstream propagation of oscillations originating from the slope-discontinuity at A. The strength of these oscillations would increase, if the angle at A is further increased to $\pi/2$. Results using the method of [12] also show the same Gibbs' phenomenon, with lesser amplitude but over a longer upstream stretch. Best results are obtained using the ORK_4 time integration strategy, as noted from the solution at $t = 900$ in Fig. 6a. Here, the Gibbs' phenomenon is virtually absent. We note that this phenomenon originates due to dispersion and phase error properties of numerical methods – as indicated by (11). In some numerical methods, the oscillations caused by dispersion magnify when they move upstream. For such cases, the dissipative nature of the basic method as given by $|G|$ can suppress Gibbs' phenomenon. On the other hand, for

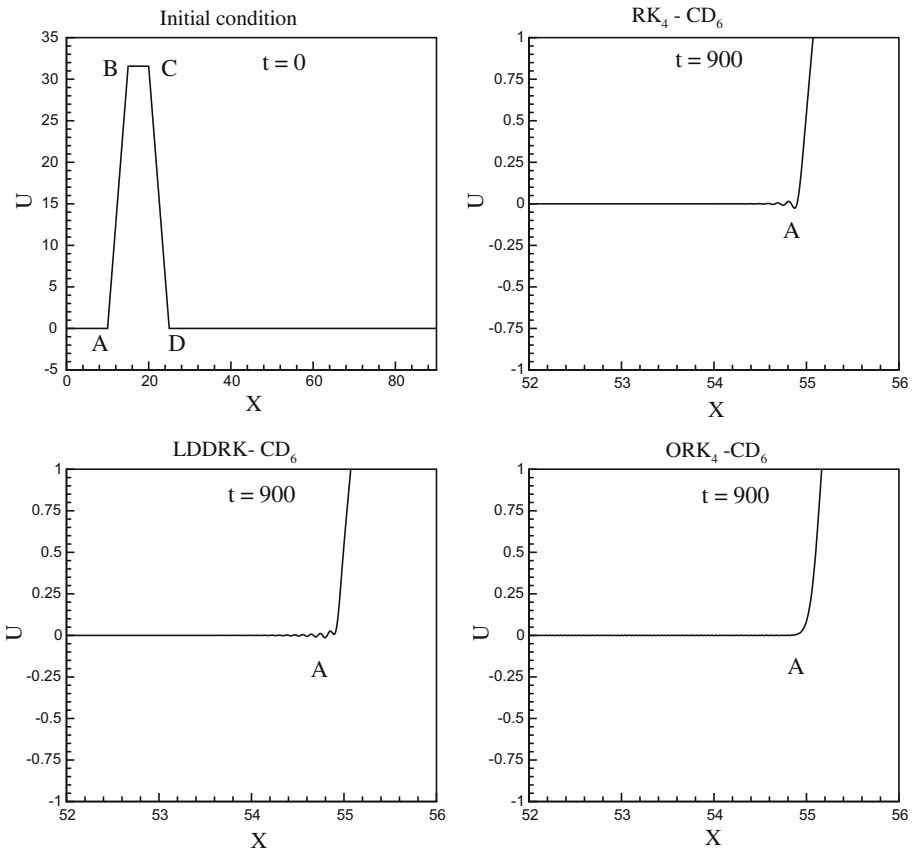

Fig. 6a. Gibbs' phenomenon for the propagation of a trapezoid-ramp function following Eq. (1), as computed by different indicated methods using $k_0h = 1.3660$ and $N_c = 0.9400$. Here, the upstream propagating wavelets originate at the left bottom point with slope discontinuity imposed via the initial condition.

a numerical method that is neutrally stable, presence or absence of Gibbs' phenomenon depends upon the phase and dispersion properties, as noted for the present $ORK_4 - CD_6$ method.

Similar such oscillations due to phase and dispersion error associated with Gibbs' phenomenon obtained at C is shown in Fig. 6b. Once again, the solutions indicate highest error for the classical RK_4 method, followed by the method of [12], while the ORK_4 method provides the most accurate result.

4. Solving 2D lid-driven cavity problem

The flow inside a square lid-driven cavity (LDC) is a benchmark problem often used to calibrate any new numerical method for solving the Navier–Stokes equations. This problem is preferred due to its definitive computational domain and unique boundary conditions. There are many papers available in the literature on this topic, but we will compare our results obtained with optimized Runge–Kutta methods with that presented in Botella and Peyret [3] and [24,25]. The results of Botella and Peyret [3] are noteworthy as these were obtained using highly accurate Chebyshev collocation spectral method. We will compare with this result for $Re = 1000$ obtained using $N = 160$ terms Chebyshev polynomial representation. While the results in [3] are for steady flow, additional validation and check for accuracy will be made for the same geometry for $Re = 10,000$, the solution of which is unsteady and shows polygonal vorticity patterns at the center of the cavity [24,25].

Before we present results of Navier–Stokes equations by ORK_3 method, we compare its numerical property in solving the wave problem with the classical RK_4 method. For both these methods, CD_4 spatial discretization has been used. One notes from the literature that CD_2 spatial discretization requires a very large number of grid points- as seen in [4] where a (1024×1024) grid was required for this flow at $Re = 1000$. In Fig. 7, we have compared the contours of $|G|$, V_{gN}/c and $(1 - c_N/c)$ for $ORK_3 - CD_4$ and $RK_4 - CD_4$ methods in solving Eq. (1). In the top frames of Fig. 7, $|G|$ contours for both the methods have been shown, from which one can see that ORK_3 method has better neutral stability property as compared to the classical RK_4 method. In the same way, the dispersion property is also better for the ORK_3 method as seen in middle frames of Fig. 7. However, the phase error for the ORK_3 method is slightly higher in comparison in terms of a critical limit for N_c. However, this error for ORK_3 is significantly lower near the origin of (kh, N_c)-plane. Moreover, this error is of lesser rel-

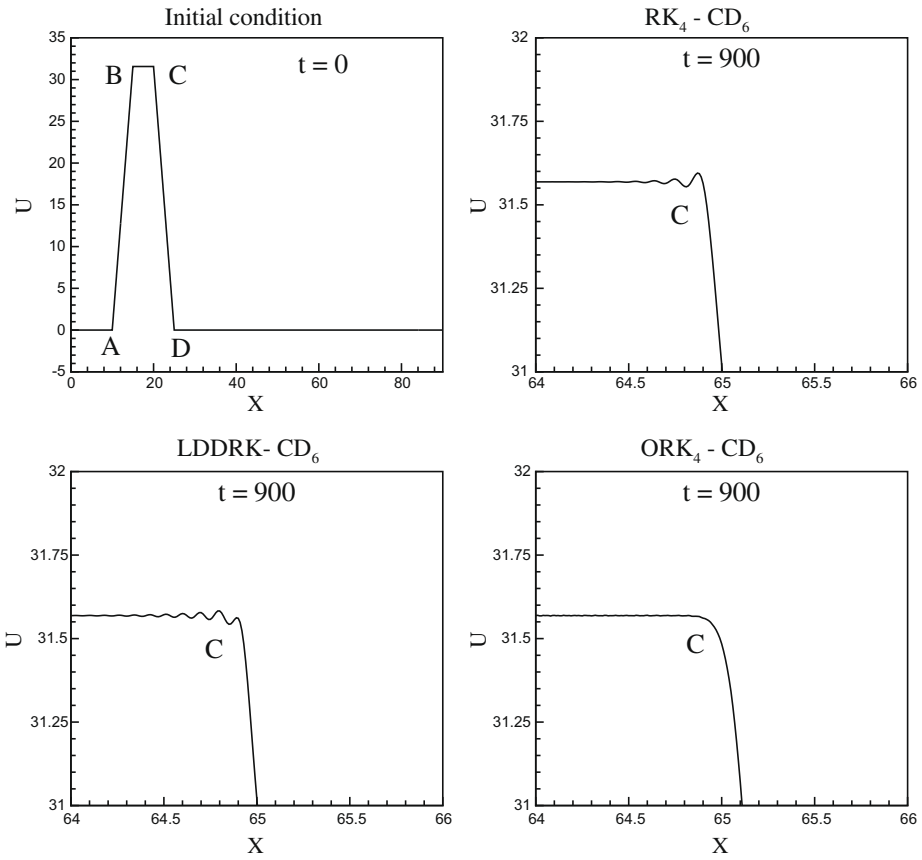

Fig. 6b. Gibbs' phenomenon for the propagation of a trapezoid-ramp function following Eq. (1), as computed by different indicated methods using $k_0h = 1.3660$ and $N_c = 0.9400$. Here, the upstream propagating wavelets originate at the top-right point with slope-discontinuity imposed via the initial condition.

evance for incompressible flow simulations. We also note that the ORK_3 method is only first order accurate as compared to the fourth order classical RK_4 method. Despite this difference in the order of the methods, ORK_3 provides lower dissipation and dispersion errors, as the process of optimization minimizes error in the spectral plane. We present the solution of incompressible Navier–Stokes equations using ORK_3 method of time discretization next.

Here the two-dimensional incompressible, viscous flow governed by the Navier–Stokes equations is solved in stream function-vorticity formulation given by,

$$\frac{\partial^2\psi}{\partial x^2}+\frac{\partial^2\psi}{\partial y^2}=-\omega \tag{41}$$

$$\frac{\partial\omega}{\partial t}+u\frac{\partial\omega}{\partial x}+v\frac{\partial\omega}{\partial y}=\frac{1}{Re}\left(\frac{\partial^2\omega}{\partial x^2}+\frac{\partial^2\omega}{\partial y^2}\right) \tag{42}$$

$$u=\frac{\partial\psi}{\partial y} \tag{43}$$

$$v=-\frac{\partial\psi}{\partial x} \tag{44}$$

where ω is the only nonzero component of the vorticity vector normal to the plane of the flow; ψ represents the stream function and (u, v) are the Cartesian components of the velocity in x and y directions, respectively. The $(\psi-\omega)$ formulation is preferred due to its inherent accuracy and computational efficiency in satisfying mass conservation exactly everywhere. We have used ORK_3 scheme for solving Eqs. (41) and (42) and to avoid errors out of mesh non-uniformities, we have used uniform grids with (751) points.

In Fig. 8, we have shown results obtained using ORK_3 and RK_4 methods of time integration for the vorticity transport equation (VTE), for $Re = 1000$ at $t = 400$. We have used the Bi-CGSTAB method [31] in solving the stream function equation and the residual convergence criteria for this is taken as 10^{-6}. The solution is advanced in time till $t = 400$ when ω is reduced to 10^{-10} i.e., till we have reached a steady state. Results showing stream function (top) and vorticity (bottom) in Fig. 8, ob-

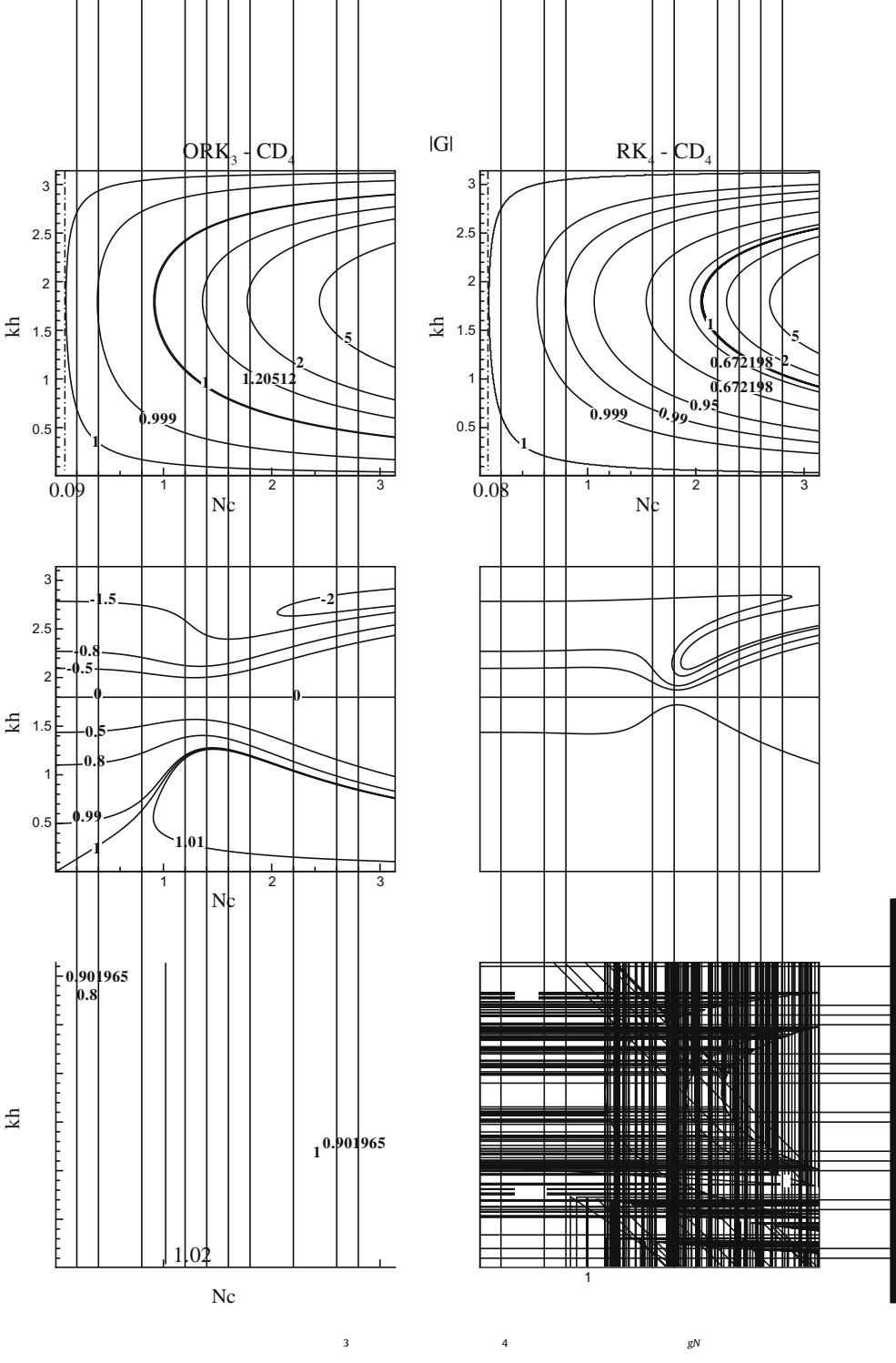

3 4 gN

tained by these time integration methods are indistinguishable. These results are quite accurate, as shown by comparing quantitatively some solution parameters in Table 1 with the results from [3,4,10]. Present results match accurately up to fourth decimal places for the maximum and minimum values of ψ in the domain. Both the time integration methods provide accurate enough results, with the ORK_3 method using only three-stages as compared to four-stages of computing with RK_4 method. Thus, one obtains more than 33 % speed-up in computing. We note that the combined compact difference (CCD) scheme of [24,25] provides results with higher accuracy, using a (256×256) grid for $Re = 10,000$. As the error in ORK_3 is less compared to RK_4 method, the convergence of the iterative solution for (41) is achieved quicker. Based on the properties shown in Fig. 7, we have taken larger time steps with the ORK_3 method. All these factors taken together, allow accelerated computations with ORK_3 by a factor of two, as compared to the RK_4 method.

While the results shown in Fig. 8 and Table 1, validate the accuracy of methods based on steady state solution, it is important to actually compare the time advancement methods for a time-dependent flow. For this reason, we have furthermore

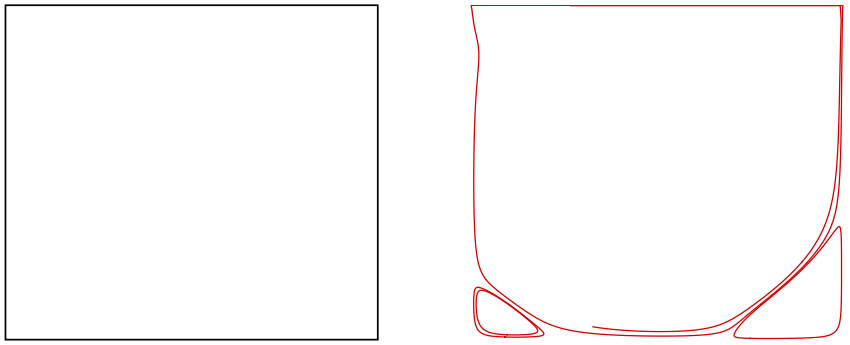

computed the LDC flow for $Re = 10,000$ using $ORK_4 - CD_4$ and $RK_4 - CD_4$ methods using a (512×512) grid and compared the results with the accurate solutions of [24,25]. The time step taken for all the computations is $\Delta t = 0.001$. The *CCD* scheme used in [24,25] is an accurate spatial discretization method with reduced error due to multiple causes, while requiring significantly fewer number of grid points. To solve the LDC flow problem for $Re = 10,000$, a grid with (257×257) points was chosen and the results were obtained using RK_4 time integration method. Results obtained using *CCD* scheme are accurate and show triangular vortex at the center of the cavity during a short interval of time. The structures appear due to forcing by (i) aliasing error caused near the top-right corner and (ii) error caused by damping (as shown by the third term on right hand side of (11)). In Fig. 9, we have shown vorticity contours obtained by three methods, as indicated in the figure. In the top frames, results are shown for the $RK_4 - CD_4$ method at $t = 1060$ and 1100. One notices rectangular vortex in the center of the cavity. But, that is damped very quickly due to numerical attenuation for the chosen $N_c = 0.5$ – as seen from Fig. 2a. In the middle frames of Fig. 9, results are shown for the same time instants obtained using the $ORK_4 - CD_4$ method. This is formally a second order accurate method, yet it provides higher accuracy due to neutral stability and lower dispersion error. In the bottom frames, results obtained by $CCD - RK_4$ method are shown. Both the frames for this method show a weak

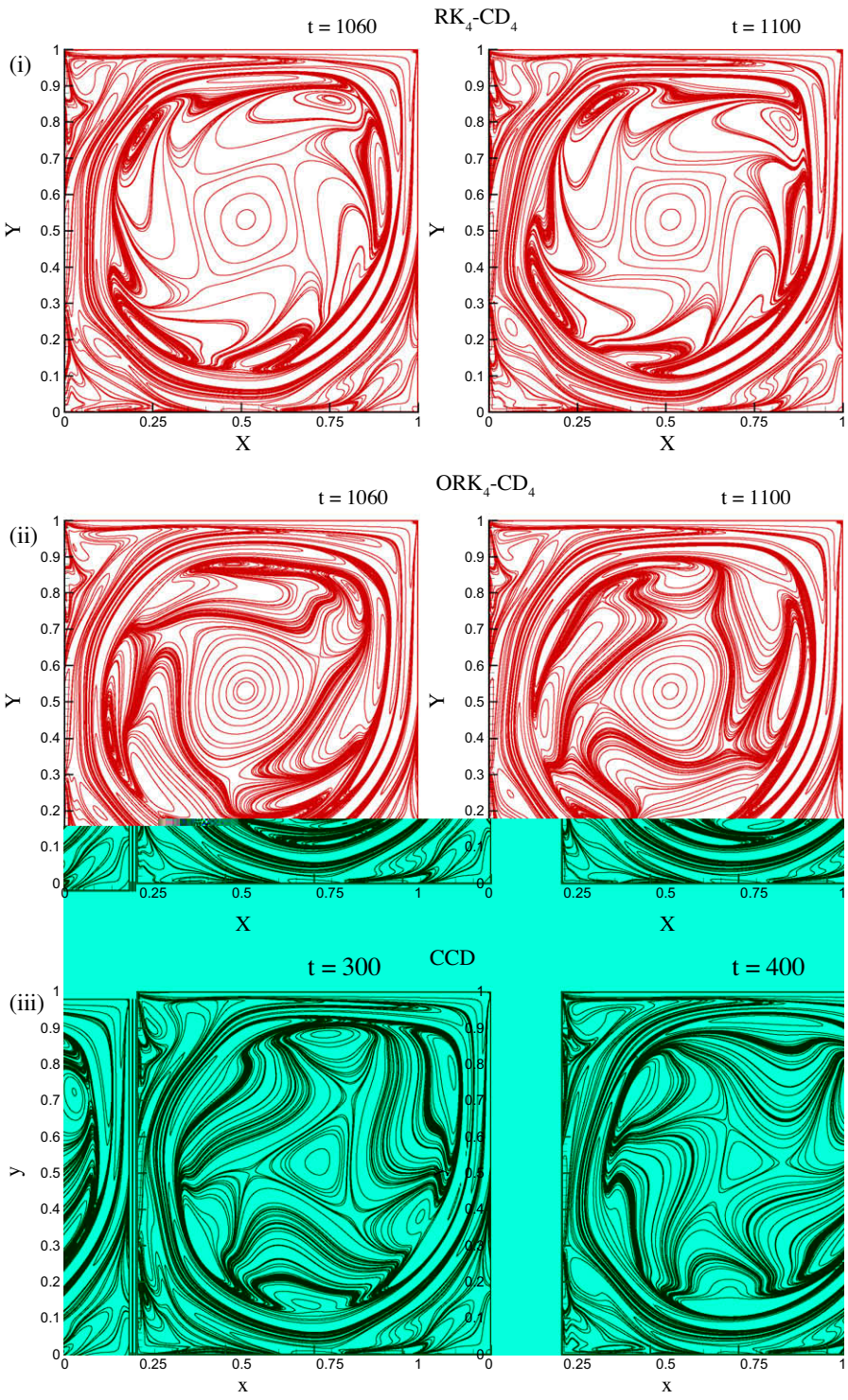

Fig. 9. Computed solution for LDC problem for $Re = 10,000$, showing vorticity contours using: (i) $RK_4 - CD_4$ scheme; (ii) $ORK_4 - CD_4$ scheme and (iii) CCD scheme due to [24,25].

triangular vortex at the center. The superior performance of $ORK_4 - CD_4$ over $RK_4 - CD_4$ method is clearly observed from the properties shown in Fig. 2a–2c. In Fig. 9, improvement of ORK_4 method is noted by noticing the similarities of the solution with that obtained by the $CCD - RK_4$ method.

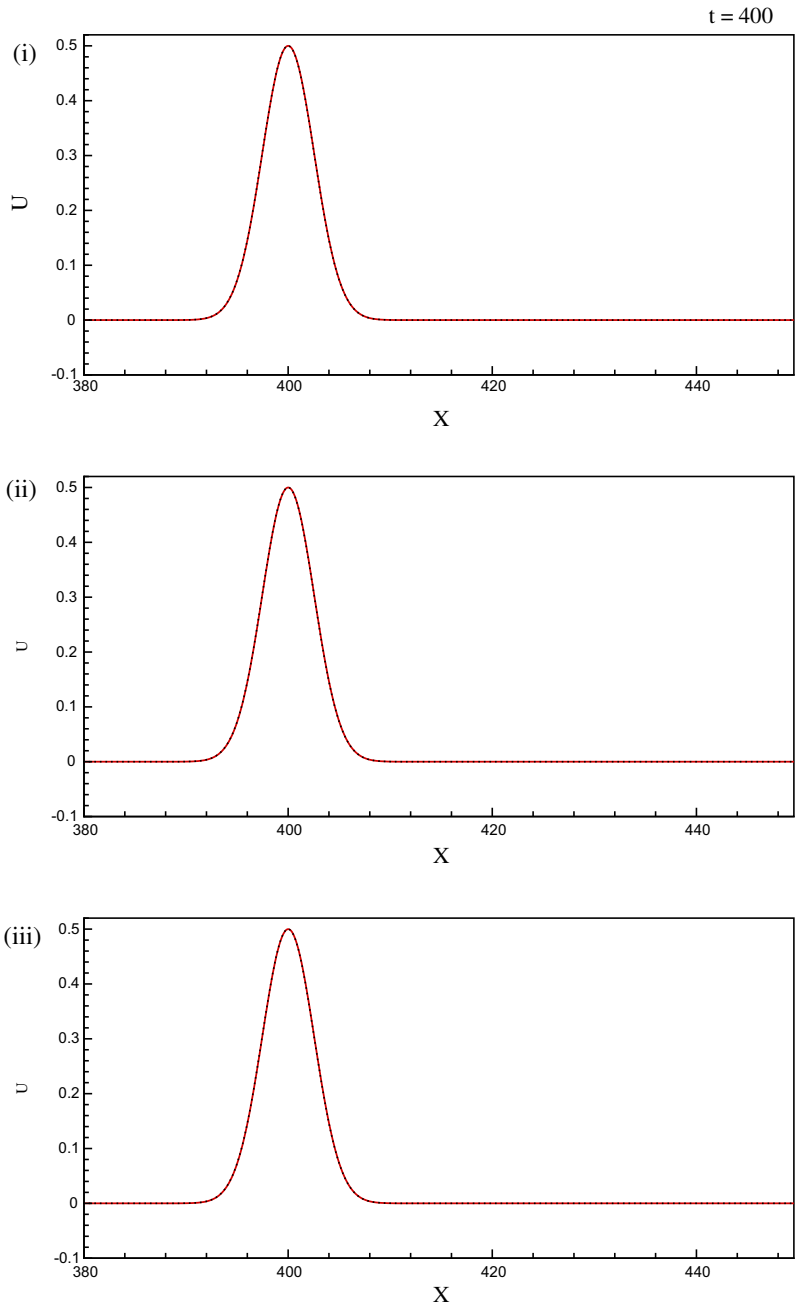

Fig. 10a. Comparison between computed (solid line) and exact (dotted line) solutions of the one-dimensional wave equation with $h = 0.1$ and $\Delta t = 0.01$ using: (i) $RK_4 - CD_4$; (ii) LDDRK [3] – CD_4 and (iii) $ORK_4 - CD_4$ schemes.

5. Benchmark problem for DRP schemes for application in CAA

This problem is taken from [29] that contains results for problems of computational aeroacoustics. The authors in [29] presented results for an initial value problem

$$\frac{\partial u}{\partial t} + \frac{\partial u}{\partial x} = 0 \tag{45}$$

that is solved subject to the initial condition given by,

$$u = 0.5\, e^{[-(\ln 2)(x/3)^2]} \tag{46}$$

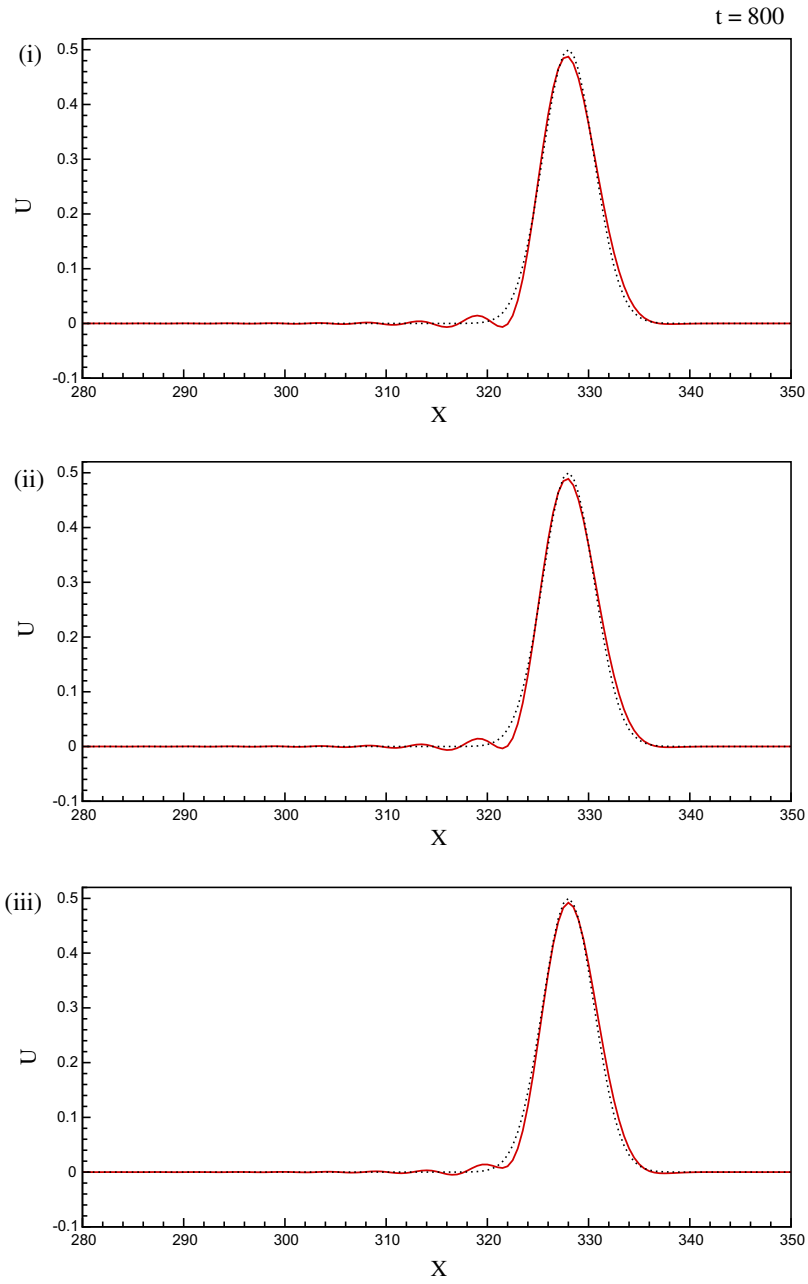

Fig. 10b. Comparison between computed (solid line) and exact (dotted line) solutions of the one-dimensional wave equation with $h = 0.5$ and $\Delta t = 0.2$: (i) $RK_4 - CD_4$; (ii) LDDRK [3] - CD_4 and (iii) $ORK_4 - CD_4$ schemes.

in the computational domain $-20 \leqslant x \leqslant 450$. In Fig. 10a, results obtained by $RK_4 - CD_4$, *LDDRK* method of [12] and $ORK_4 - CD_4$ with the computational parameters given by $h = 0.1$ and $\Delta t = 0.01$ are compared with exact solution and among themselves. For these computational parameters, all the three methods show results that are indistinguishable from the exact solution. When we performed another set of calculations shown in Fig. 10b using $h = 0.5$ and $\Delta t = 0.2$, the computed solutions show some differences. For example, results obtained by the classical $RK_4 - CD_4$ method show Gibbs' phenomenon at the foot of the wave-packet on the upstream side. These spurious oscillations correspond to $kh \geqslant 1.8$ for the properties shown in Fig. 2b. Same kind of upstream propagating waves are predicted for all the three methods with the same onset value of $kh = 1.8$. The difference among the upstream part of the three computed solutions can be explained from the $|G|$ contours shown in Fig. 2a. These upstream propagating waves are created due to numerical error. For the classical $RK_4 - CD_4$ method, this numerical error for $N_c = 0.4$ is due to numerical attenuation. For the *LDDRK* method, the numerical

error for the same N_c is due to mild instability (as seen in Fig. 2a). In comparison to these two methods, the proposed $ORK_4 - CD_4$ method is neutrally stable across all kh range for this N_c. Absence of input via numerical error for the $ORK_4 - CD_4$ method is responsible for lesser Gibbs' phenomenon. However, for all the three methods, one notices a very small amount of dispersion of the solution at large time, $t = 800$.

6. Conclusion

In the present work, we have proposed new Runge–Kutta temporal discretization schemes by optimizing the classical two-stage, second order (RK_2); three-stage, third order (RK_3) and four-stage, fourth order (RK_4) schemes coupled with central difference schemes for spatial discretization subject to constraints on neutral numerical amplification factor, minimal dispersion and phase errors in solving one-dimensional convection equation. These methods have been compared with other optimized time integration methods reported in [1,6,12,15,17]. In these methods, the objective function is designed to minimize the difference between numerical and "exact" amplification factor. The difference of the present methods from others is due to the requirement of satisfying constraints that originate from the actual error propagation equation (Eq. (11)). Since the attempt is on reducing error by considering spatial and temporal discretization schemes together, this gives rise to true DRP schemes. Such schemes are suitable for convection dominated flows and problems of acoustics.

The schemes proposed are of lower order due to the imposition of constraints on neutral stability, dispersion and phase error. For example, ORK_2 and ORK_3 schemes obtained from classical two-stage and three-stage explicit Runge–Kutta methods, are nominally first order accurate, but provide larger allowable time steps. Numerical properties in Figs. 2 and 3 establish the superiority of the proposed Runge–Kutta schemes in satisfying neutral stability and lower dispersion error. The $ORK_4 - CD_4$ method has the largest continuous range in (kh, N_c) -plane where the method is neutrally stable as seen from Fig. 2a. This is followed by the methods in [6] and [1,15]. In contrast, methods of [12,17] looks similar to classical $RK_4 - CD_4$ method. The dispersion property in Fig. 2b is seen to be the best for the $ORK_4 - CD_4$ method followed by the LDDRK method [12], with other methods showing no improvements over the classical method. The optimized methods for CD_6 spatial discretization, exhibit the best neutral stability property as compared to other methods involving four- and six-stage schemes. The next best set of results are for the classical RK_6 method and that due to [1,15], as seen in Fig. 3b. It is noted that increase of spatial discretization accuracy results in further improvement of dispersion property.

The improvements which have been achieved in the work are as follows:

(1) Better neutral stability property of the ORK methods is demonstrated for the propagation of a wave-packet as compared with LDDRK schemes [12] and the classical RK_4 method in Fig. 4a–4c. The LDDRK method [12] is slightly unstable and another scheme from [12] based on using a combination of four- and six-stage RK_4 method is studied and results shown in Fig. 4b(ii).

(2) DRP property of the optimized schemes are also compared with the same wave-packet propagation case, computed with different numerical parameters and the results are shown in Fig. 5a–5c. The classical $RK_4 - CD_6$ method experiences large dissipation with negligible dispersion. In Fig. 5b, results obtained by two methods of [12] are shown. For the four-stage LDDRK method, results show larger dissipation as compared to the two-step alternating RK_4 time integration schemes. Results shown in Fig. 5c obtained using $ORK_4 - CD_6$ method show zero dispersion and significantly lower attenuation.

(3) The effectiveness of the optimized schemes are compared, by solving Navier–Stokes equations for the flow in a square lid-driven cavity for $Re = 1000$ with $ORK_3 - CD_4$ and $RK_4 - CD_4$ methods, in Fig. 8. The speed-up of the $ORK_3 - CD_4$ method over the $RK_4 - CD_4$ method is obtained due to fewer stages of computations and better error properties that allows taking larger time steps. All these taken together accelerate computation by a factor of at least two. Furthermore, better DRP property of the optimized schemes is shown by solving unsteady LDC flow for $Re = 10,000$ using $ORK_4 - CD_4$ and $RK_4 - CD_4$ schemes. The results are compared with that reported in [24,25] in Fig. 9. It is noted that the $ORK_4 - CD_4$ is superior to $RK_4 - CD_4$ method in capturing polygonal vortical structures in the core of the cavity [24,25].

(4) We have also solved the initial value problem (Eqs. (45) and (46)) [29], for the propagation of a wave-packet using $RK_4 - CD_4$, LDDRK [3] – CD_4 and $ORK_4 - CD_4$ schemes and compared the results with exact solution. Results in Fig. 10a are indistinguishable for the chosen h and Δt. When h and Δt are increased, results obtained by the classical $RK_4 - CD_4$ and LDDRK [12] – CD_4 methods show Gibbs' phenomenon on the upstream side, as shown in Fig. 10b. The $ORK_4 - CD_4$ method shows Gibbs' phenomenon less compared to other schemes.

The parameters a and b in (26) and (27) for the optimized Runge–Kutta methods have been chosen here for large values of N_c where these do not vary appreciably. There are possibilities of improving the scheme, by obtaining exact values of a and b for the exact CFL number.

References

[1] M. Bernardini, S. Pirozzoli, A general strategy for the optimization of Runge–Kutta schemes for wave propagation phenomena, J. Comput. Phys. 228 (2009) 4182–4199.

[2] C. Bogey, C. Bailly, A family of low dispersive and low dissipative explicit schemes for flow and noise computations, J. Comput. Phys. 194 (2004) 194–214.
[3] O. Botella, R. Peyret, Benchmark spectral results on the lid-driven cavity flow, Comput. Fluids 27 (4) (1998) 421–433.
[4] C.-H. Bruneau, M. Saad, The 2D lid-driven cavity problem revisited, Comput. Fluids 35 (2006) 326–348.
[5] J.C. Butcher, The Numerical Analysis of Ordinary Differential Equations, Runge–Kutta and General Linear Methods, Wiley, New York, 1987.
[6] M. Calvo, J.M. Franco, L. Randez, A new minimum storage Runge–Kutta scheme for computational acoustics, J. Comput. Phys. 201 (2004) 1–12.
[7] J.G. Charney, R. Fjortoft, J. von Neumann, Numerical integration of the barotropic vorticity equation, Tellus 2 (1950) 237–254.
[8] J. Crank, P. Nicholson, A practical method for numerical evaluation of solutions of partial differential equations of the heat conduction type, Proc. Camb. Philol. Soc. 43 (1947) 50–67.
[9] A. Dipankar, T.K. Sengupta, Symmetrized compact scheme for receptivity study of 2D transitional channel flow, J. Comput. Phys. 215 (1) (2006) 245–253.
[10] U. Ghia, K.N. Ghia, C.T. Shin, High-Re solution for incompressible flow using the Navier–Stokes equations and a multigrid method, J. Comput. Phys. 48 (1) (1982) 387–411.
[11] Z. Haras, S. Ta'asan, Finite difference scheme for long time integration, J. Comput. Phys. 114 (1994) 265–279.
[12] F.Q. Hu, M.Y. Hussani, J.L. Manthey, Low-dissipation and low-dispersion Runge–Kutta schemes for computational acoustics, J. Comput. Phys. 124 (1996) 177–191.
[13] M.K. Jain, S.R.K. Iyengar, R.K. Jain, Numerical Methods for Scientific and Engineering Computation, New Age International Publishers, New Delhi, 2007.
[14] S.K. Lele, Compact finite difference schemes with spectral-like resolution, J. Comput. Phys. 103 (1992) 16–42.
[15] S. Pirozzoli, Performance analysis and optimization of finite-difference schemes for wave propagation problems, J. Comput. Phys. 222 (2007) 809–831.
[16] A. Ralston, A First Course in Numerical Analysis, McGraw Hill Book Co., New York, 1965.
[17] J. Ramboer, T. Broeckhoven, S. Smirnov, C. Lacor, Optimization of time integration schemes coupled with spatial discretization for use in CAA applications, J. Comput. Phys. 213 (2006) 777–802.
[18] T.K. Sengupta, G. Ganeriwal, S. De, Analysis of central and upwind schemes, J. Comput. Phys. 192 (2) (2003) 677–694.
[19] T.K. Sengupta, Fundamentals of Computational Fluid Dynamics, Universities Press, Hyderabad, India, 2004.
[20] T.K. Sengupta, A. Dipankar, A comparative study of time advancement methods for solving Navier–Stokes equations, J. Sci. Comput. 35 (2) (2004) 225–250.
[21] T.K. Sengupta, G. Ganeriwal, A. Dipankar, High accuracy compact scheme and Gibb's phenomenon, J. Sci. Comput. 21 (3) (2004) 253–268.
[22] T.K. Sengupta, S.K. Sircar, A. Dipankar, High accuracy schemes for DNS and acoustics, J. Sci. Comput. 26 (2) (2006) 151–193.
[23] T.K. Sengupta, A. Dipankar, P. Sagaut, Error dynamics: beyond von Neumann analysis, J. Comput. Phys. 226 (2007) 1211–1218.
[24] T.K. Sengupta, V. Lakshmanan, V.V.S.N. Vijay, A new combined stable and dispersion relation preserving compact scheme for non periodic problems, J. Comput. Phys. 228 (2009) 3048–3071.
[25] T.K. Sengupta, V.V.S.N. Vijay, S. Bhaumik, Further improvement and analysis of CCD scheme: dissipation discretization and de-aliasing properties, J. Comput. Phys. 228 (2009) 6150–6168.
[26] Yu.I. Shokin, The Method of Differential Approximation, Springer-Verlag, Berlin, 1983.
[27] D. Stanescu, W.G. Habashi, 2N-storage low dissipation and dispersion Runge–Kutta schemes for computational acoustics, J. Comput. Phys 143 (1998) 674–681.
[28] C.K.W. Tam, J.C. Webb, Dispersion-relation preserving finite difference schemes for computational acoustics, J. Comput. Phys. 107 (1993) 262–281.
[29] C.K.W. Tam, H. Shen, K.A. Kurbatskii, L. Auriault, Z. Dong, J.C. Webb, in: ICASE/LaRC Workshop on Benchmark Problems in Computational Aeroacoustics (CAA), vol. 149, 1995.
[30] L.N. Trefethen, Group velocity in finite difference schemes, SIAM Rev. 24 (2) (1982) 113–136.
[31] H.A. Van Der Vorst, Bi-CGSTAB: a fast and smoothly converging variant of Bi-CG for the solution of nonsymmetric linear systems, SIAM J. Sic. Stat. Comput. 13 (2) (1992) 631–644.
[32] R. Vichnevetsky, J.B. Bowles, Fourier analysis of numerical approximations of hyperbolic equations, SIAM Stud. Appl. Math., vol. 5, SIAM, Philadelphia, USA, 1982.
[33] R. Warming, R. Hyett, The modified equation approach to the stability and accuracy analysis of finite difference methods, J. Comput. Phys. 14 (1974) 159–179.